UNIVERSIDADE FEDERAL DO RIO GRANDE
PÓS-GRADUAÇÃO EM OCEANOGRAFIA FÍSICA, QUÍMICA E GEOLÓGICA

DISTRIBUIÇÃO DOS FLUXOS LÍQUIDOS DE CO_2 NA LATITUDE DE 35°S DO OCEANO ATLÂNTICO E PLATAFORMAS CONTINENTAIS ADJACENTES

JANNINE MARQUEZ LENCINA AVILA

Dissertação apresentada ao Programa de Pós-Graduação em Oceanografia Química, Física e Geológica do Instituto de Oceanografia da Universidade de Rio Grande como requisito parcial à obtenção do título de MESTRE.

Orientador: Prof. Dr. Carlos A. E. Garcia
Co-Orientadora: Dra. Rosane G. Ito

RIO GRANDE
2014

SUMÁRIO

LISTA DE FIGURAS

LISTA DE TABELAS

LISTA DE ACRÔNIMOS

BC – Corrente do Brasil

BCLME – Ecossistema marinho da corrente de Benguela

BgC – Corrente de Benguela

GLM – Modelo linear generalizado

MC – Corrente das Malvinas

mSTSW – Água Subtropical de Superfície modificada

PLW – Água da Pluma da lagoa dos Patos

PPW – Água da Pluma do Prata

SAC – Corrente do Atlântico Sul

SACW – Água Central do Atlântico Sul

STSW – Água Subtropical de Plataforma

TW – Água Tropical

RESUMO

Os níveis de CO_2 atmosférico atingiram valores acima de 400 ppm durante este ano. Os oceanos atuam de forma importante na absorção desse CO_2 atmosférico, embora, regiões como o oceano Atlântico Sul continuam subamostradas. Neste estudo determinou-se o comportamento, em termos de fluxo de CO_2, deste oceano ao longo da latitude de 35°S e plataformas adjacentes durante período de primavera e início do verão. Dados de fração molar de CO_2, temperatura, salinidade e oxigênio foram amostrados continuamente. Dados discretos de concentração de clorofila-a foram utilizados como dado suporte. Valores de fugacidade de CO_2 na superfície do mar, fCO_2^{sw}, (335.9 ± 9.6) e ΔfCO_2 (diferença entre fugacidade do CO2 na superfície da água do mar e na atmosfera) demonstraram alta variabilidade ao longo de todo o cruzeiro, sendo que as principais variações encontraram-se nas regiões de plataforma e talude continentais. Todos os valores de ΔfCO_2^{sw} foram negativos (-49.0 ± 9.9), demonstrando que toda a região de estudo comportou-se como sumidouro de CO2 atmosférico. O fluxo líquido médio para todo o cruzeiro de -3,1 ± 2,2 mmol m^{-2} d^{-1} (velocidade de transferência, Wanninkhof 1992). Temperatura e salinidade foram os principais fatores influentes sobre fCO_2^{sw}, e a clorofila-a demonstrou pouca contribuição para todo o cruzeiro. Algoritmos para previsão de fCO_2^{sw} e fCO_2^{sw} normalizado foram desenvolvidos para as três sub-regiões identificadas neste estudo: regiões sul-americana, oceânica e africana. Os modelos de previsão para o fCO_2 normalizado mostraram os melhores resultados, especialmente na porção oeste (Brasil até 20°W) da região de estudo.

Palavras Chave

Fugacidade do CO_2, Oceano Atlântico Sul Subtropical, plataforma continental, fluxo líquido de CO_2

ABSTRACT

Atmospheric CO_2 reached levels above 400 ppm during 2014. The oceans play an important role in absorbing this atmospheric CO_2 increase, but several oceanic regions, such as the South Atlantic Ocean, are undersampled. This study assessed the ocean's behavior along the latitude of 35°S and adjacent shelves during spring 2011 and early summer periods. Underway CO_2 molar fraction, temperature, salinity and dissolved oxygen were taken continuously from Brazil to Africa. Satellite and discrete chlorophyll concentration along the ship's track were used as support data. Sea-surface CO_2 fugacity (fCO_2^{sw}) and difference in sea-air CO_2 fugacity (ΔfCO_2^{sw}) showed high variability for the entire cruise, with higher values on continental shelf and slope regions. All ΔfCO_2^{sw} values were negative, meaning that a sink process was occurring during the cruise period and yielding a net CO_2 flux of -3.1 ± 2.2 mmol m^{-2} day^{-1} for the entire cruise (using Wanninkhof 1992). Surface temperature and salinity were the main contributors to fCO_2^{sw} variability with chlorophyll showing little contribution for the whole cruise. Algorithms for fCO_2 and normalized fCO_2 were developed for the South American coastal, oceanic and African regions. The normalized fCO_2 o models presented better results, specially in the western portion (Brazil to 20° W) of the study area.

Key words

CO_2 fugacity, Subtropical South Atlantic Ocean, continental shelf, sea-air CO_2 flux

ESTRUTURA DA DISSERTAÇÃO

Para obtenção do título de Mestre, pelo Programa de Pós-Graduação em Oceanografia Física, Química e Geológica, requer-se a submissão de um artigo científico, tendo como primeiro autor o candidato a mestre, para publicação em periódico com corpo indexado. Sendo assim, os resultados da pesquisa científica, desenvolvida durante o mestrado, serão apresentados no artigo, redigido em inglês, no corpo da dissertação.

Este documento esta subdividido em cinco seções. Na 1ª seção, faz-se uma introdução ao assunto, descrição da região de estudo e revisão bibliográfica, levando aos objetivos do presente estudo. A 2ª seção apresenta a metodologia, descrevendo a obtenção dos dados, métodos utilizados para se obter o fluxo líquido de CO_2, bem como, as análises de contribuição dos processos biológicos e físicos, e modelos de previsão de fCO_2. Na 3ª seção, encontra-se o manuscrito a ser submetido para publicação, redigido em inglês onde procurou-se incluir os resultados mais importantes, a discussão e as considerações finais. A 4ª seção apresenta a síntese dos resultados apresentados no manuscrito. Na 5ª e última seção, estão as conclusões do estudo

INTRODUÇÃO

1. INTRODUÇÃO

1.1. OCEANOS E AQUECIMENTO GLOBAL

As concentrações de CO_2 atmosférico atingiram níveis nunca antes registrados nos últimos 800.000 anos (Luthi *et al.* 2008; IPCC 2013). No período pré-industrial, estes valores eram, aproximadamente, 280 ppm para a fração molar de ar seco (quantidade em µmol deste gás por mol de todos os gases na atmosfera, após o vapor de água ser removido) do CO_2 atmosférico. Em 2014, os níveis atingiram 401,8 ppm no mês de maio na estação de Mauna Loa, no hemisfério Norte, valor este que corresponde a mais de 40% sobre aqueles pré-industriais (Tans & Keeling 2014). Além disso, o último relatório do IPCC (2013) confirmou a influência antrópica como fator para o aquecimento global observado desde a metade do século XX devido, principalmente, à queima de combustíveis fósseis, mudança no uso da terra, produção de cimento e desmatamento de florestas. As consequências desta influência têm sido detectadas no aquecimento da atmosfera e dos oceanos, em mudanças no ciclo global da água, nas reduções de neve e de gelo, na elevação do nível médio do mar e em mudanças de eventos climáticos extremos (Le Quéré *et al.* 2009; IPCC 2013). Ainda assim, níveis de CO_2 atmosférico ainda mais altos poderiam ser alcançados se os oceanos e a biosfera terrestre não absorvessem parte dessas emissões. Juntos, a biosfera terrestre e os oceanos são responsáveis pela absorção de aproximadamente 50% do CO_2 atmosférico (Schimel *et al.* 2001), sendo os oceanos um dos componentes principais no sequestro do CO_2 atmosférico (Sabine *et al.* 2004). Com base no estudo do conjunto de dados do balanço global do carbono, obtidos entre 2003 e 2012, estima-se que os oceanos já absorveram cerca de 2,6 ± 0,5 Pt C ano^{-1} (Le Quéré *et al.* 2013).

A absorção do CO_2 atmosférico pelos oceanos ocorre através de dois processos, conhecidos como (1) bomba de solubilidade ou física e (2) bomba biológica (Cox *et al.* 2000, Libes 2009). O primeiro processo é governado por processos físicos associados à solubilidade do gás e à circulação da água. De uma forma geral, os gases são mais solúveis em ambientes com temperaturas mais baixas. Dessa forma, em regiões de altas latitudes, o dióxido de carbono apresenta o dobro de solubilidade do que em regiões de baixas latitudes. A eficiência da bomba de **termodinâmica** é controlada por três fatores: (i) o efeito da temperatura, (ii) o movimento físico da água do mar e (iii) as reações químicas que o gás CO_2 sofre ao entrar em contato com a água do mar (Millero 2007, Dickson 2007). O segundo processo é regido pela atividade fitoplanctônica e pode ser separado em dois estágios. Primeiramente, o fitoplâncton assimila o CO_2 dissolvido ao realizar a fotossíntese, transformando-o em matéria orgânica ou carbono orgânico particulado (*Particulate Organic Carbon* – POC) e carbono inorgânico particulado (*Particulate Inorganic Carbon* – PIC) na forma de esqueletos ou carapaças. Estes são, então, transportados para profundidades logo abaixo da termoclina através de processos de advecção e mistura verticais. No segundo

estágio, todo POC e PIC não remineralizado submerge até o fundo oceânico, onde será sedimentado (Tsunogai *et al.* 1999; Libes 2009; Gregon & Monteiro 2013).

Os processos de troca de CO_2 na interface oceano-atmosfera levam a alterações na fugacidade (a pressão parcial do CO_2 corrigida por não ser um gás ideal) deste gás na água do mar. Na atmosfera, a pressão parcial do CO_2 é o produto entre a fração molar do CO_2 e a pressão atmosférica do ar seco, seguindo a Lei dos Gases Ideais (Dickson 2007, Libes 2009). Quando dissolvido na água do mar, o gás CO_2 segue a Lei de Henry em que a pressão parcial de um gás é diretamente proporcional à concentração desse gás em sua fase aquosa e inversamente proporcional à sua solubilidade, que por sua vez varia conforme a temperatura e a salinidade (Libes 2009). Os oceanos apresentam maior variabilidade, principalmente espacial, das concentrações de CO_2 e consequentemente da fugacidade do CO_2 (fCO_2), do que a atmosfera, devido ao maior dinamismo dos processos oceânicos, como, por exemplo, correntes, vórtices, frentes oceânicas e costeiras. Sendo assim, o oceano é o principal controlador dos fluxos de CO_2 na interface oceano-atmosfera (Takahashi *et al.* 2009).

O fluxo líquido de CO_2 na interface oceano-atmosfera é determinado por uma taxa de transferência do CO_2 nesta interface, pelo coeficiente de solubilidade do CO_2 e, principalmente, pela diferença entre as pressões parciais do CO_2 no oceano e na atmosfera (Takahashi *et al.* 2002). A taxa de transferência do gás depende da velocidade do vento, sendo que vários trabalhos apresentam distintas relações entre a velocidade do vento e o fluxo do gás (e.g. Liss & Merlivat 1986, Wanninkhof 1992, Wanninkhof & McGillis 1999, Nightingale *et al.* 2000, Ho *et al.* 2006, Takahashi *et al.* 2009).

Desde a segunda metade da década de 90, Takahashi *et al.* (1997) já apresentavam estimativas globais de fluxos líquidos de CO_2 variando entre 0.60–1.34 Pt C ano^{-1} e indicavam o oceano Atlântico Sul como o mais importante sumidouro de CO_2 atmosférico com 60% da absorção global. A maioria dos trabalhos concentrou-se no hemisfério norte e nas regiões equatoriais dos oceanos. A última climatologia global de Takahashi *et al.* (2009) estimou que os oceanos absorveram 2.0 ± 1.0 Pg C ano^{-1} em 2000, sendo que os oceanos em latitudes médias são os principais sumidouros de CO_2 (-0.70 Pg C ano^{-1}, para o hemisfério norte, e -1.05 Pg C ano^{-1}, para o hemisfério sul). Contudo, ainda existem regiões pouco amostradas, sendo o oceano Atlântico Sul uma delas (Takahashi *et al.* 2009). Na última década, porém, avançou-se nos estudos do sistema carbonato com o aumento de regiões amostradas, em especial nas regiões de plataforma continental (e.g. Bozec *et al.* 2005, Ito *et al.* 2005, Jiang *et al.* 2008, Bianchi *et al.* 2005, 2009, Chen & Borges 2009; Lefèvre 2009, González-Dávila *et al.* 2009; Santana-Casiano *et al.* 2009).

Tsunogai *et al.* (1999) propôs o conceito da bomba em plataformas continentais (c*ontinental shelf pump*), em que a menor temperatura da plataforma interna, associada a alta produtividade primária, aumentariam a absorção de CO_2 pela superfície marinha, sendo posteriormente, remineralizado no fundo e exportado por transportes de mistura isopicnais. Esta bomba seria

responsável pela absorção de 1 Pg C ano^{-1} se todas as zonas costeiras tivessem a mesma taxa de absorção que a plataforma continental do mar do Leste da China. Numa primeira tentativa de integrar os fluxos líquidos de CO_2 em zonas costeiras, Borges (2005) estimou a contribuição dos oceanos costeiros na absorção de CO_2 atmosférico, considerando-os como sumidouros (-0.53 Pg C m^{-2} ano^{-1}) quando estuários e mangues não são considerados no cálculo, e fontes de CO_2 para a atmosfera (0.12 Pg C m^{-2} ano^{-1}) se consideradas estas zonas de plataforma interna. Cai *et al.* (2006), baseados em dados mais heterogêneos e abrangentes, estimaram que plataformas continentais de baixas latitudes também atuam como fontes de CO_2 para a atmosfera (0.11 Pg C ano^{-1}) e plataformas de média-altas latitude como fracos sumidouros (-0.33 Pg C ano^{-1}). A revisão de Chen & Borges (2009) mostra uma visão diferente, determinando plataformas continentais como sumidouros (-0.33 a -0.36 Pg C ano^{-1}), e ecossistemas próximos à costa como fontes (0.50 Pg C ano^{-1}). Além disso, a região sudoeste do oceano Atlântico Sul, influenciada pela Corrente do Brasil foi considerada sumidouro (-0.07 Pg CO_2 ano^{-1}), enquanto que a borda sudeste, influenciada pela Corrente de Benguela, foi designada como fonte (0.005 Pg CO_2 ano^{-1}). Recentemente, Laruelle *et al.* (2010) determinaram os sistemas de ressurgência na zona temperada do Atlântico como sumidouros de CO_2 (-0.02 ± 0.001 Pg C ano^{-1}), contrários aos sistemas do Pacífico e Índico para a mesma banda de latitude (0.011 ± 0.008 e 0.001 ± 0.002 Pg C ano^{-1}, respectivamente) e, ainda, que as regiões plataforma aberta em regiões temperadas apresentam um fluxo líquido de CO_2 entre atmosfera-mar igual a -0.086 ± 0.087 Pg C ano^{-1} (Laruelle *et al.* 2010).

Regiões costeiras, tanto de borda leste, como de borda oeste, são caracterizadas pela alta dinâmica de processos físicos e biogeoquímicos devido à sua interação com o continente adjacente (Chen & Borges 2009; Laruelle *et al.* 2010). Entretanto, apesar de sua importância frente aos processos que podem regular os fluxos líquidos de CO_2, bem como o transporte de CO_2 para outras camadas inferiores do oceano, estas regiões ainda estão subquantificadas (Borges *et al.* 2005; Monteiro 2010). Consequentemente, a troca de CO_2 na interface oceano-atmosfera nas margens costeiras não é devidamente representada em modelos atuais do ciclo global do carbono, nem nas medidas *in situ* da pCO_2/fCO_2 globais, usados em estudos climatológicos (Orr *et al.* 2001; Sarmiento & Gruber 2002; Takahashi *et al.* 2009).

1.2. ÁREA DE ESTUDO

A região de estudo (Figura 1) abrange a porção sul do giro subtropical do oceano Atlântico Sul, compreendendo a região oceânica ao longo da latitude de 35°S e as plataformas continentais do Uruguai e sul do Brasil, no Atlântico ocidental, e a plataforma continental do sul da África, no Atlântico oriental. Nesta região, a circulação geral do giro (Figura 1) é formada pela Corrente do Brasil (*Brazil Current* – BC), como corrente de contorno oeste, a Corrente do Atlântico Sul (*South*

Atlantic Current – SAC), como limite sul do giro, e a Corrente de Benguela (*Benguela Current* – BgC), como corrente de contorno leste (Peterson & Stramma 1991).

A região das plataformas uruguaia e do sul do Brasil apresenta alta dinâmica e variabilidade (sazonal e interanual), pois sofre grande influência da Água da Pluma do Rio da Prata (*Plata Plume Water* – PPW) e da Água da Pluma da Lagoa dos Patos, esta última em menor quantidade, sendo ambas consideradas como PPW por Möller *et al.* (2008). A PPW pode alcançar latitudes de 28°S durante o inverno por influência dos ventos de S/SW dominantes durante esta estação (Möller *et al.* 2008). No verão, entretanto, com a mudança dos ventos para N/NE, a pluma se retrai para latitudes de até 32°S, espalhando-se ao longo da plataforma, podendo atingir a quebra da plataforma. A PPW forma uma capa superficial sobre as massas de Água Tropical e Central do Atlântico Sul que estão sobre a plataforma continental (Möller *et al.* 2008). Na quebra de plataforma, a BC flui em direção ao Sul até cerca de 38°S quando encontra a Corrente das Malvinas (*Malvinas Current* – MC). Nesta região de alta dinâmica, conhecida como Confluência Brasil-Malvinas, ambas as correntes migram para leste, meandrando em direção ao oceano aberto, formando a SAC (Stramma & England 1999).

As plataformas uruguaia e do sul do Brasil apresentam alta produtividade biológica, que está relacionada com as descargas do Rio da Prata, primeiramente, e do estuário da Lagoa dos Patos em menor escala (Muelbert *et al.* 2008). Ainda, a interação entre águas de plataforma (subtropical e subantártica) da região com águas oceânicas, como a Água Central do Atlântico Sul, que pode subir à plataforma através de processes de mesoescala, também influencia a produtividade primária, bem como a concentração de nutrientes, sendo que a produtividade primária na região pode chegar a 160 g C m^{-2} ano^{-1} (Odebrecht & Garcia 1997).

Na plataforma continental do sudoeste da África, localiza-se o Sistema de Ressurgência da Corrente de Benguela (*Benguela Current Large Marine Ecosystem* – BCLME), localizado entre 5°S-37°S e 0-26°E. Este sistema abriga um dos quatro ecossistemas de ressurgência de borda leste mais importantes do planeta, responsável por uma alta produtividade biológica (Monteiro 2010). Entre 15-37°S, as correntes superficiais são predominantemente em direção ao equador, com intensas células de ressurgência costeira e jatos de quebra de plataforma estreitos, próximos à Cidade do Cabo (34°S, 18°E) e Lüderitz (28°S, 15°E). Esta região mais ao sul do BCLME (30-34°S) apresenta ressurgência sazonal que ocorre durante o verão (Shillington *et al.* 2006). A região oceânica adjacente é conhecida pela alta incidência de vórtices gerados pela retroflexão das Agulhas e pelo vazamento da Corrente das Agulhas, de forma que a grande maioria de vórtices incidentes é do tipo anti-ciclônico (núcleo quente e menos produtivas) (Gordon *et al.* 1987).

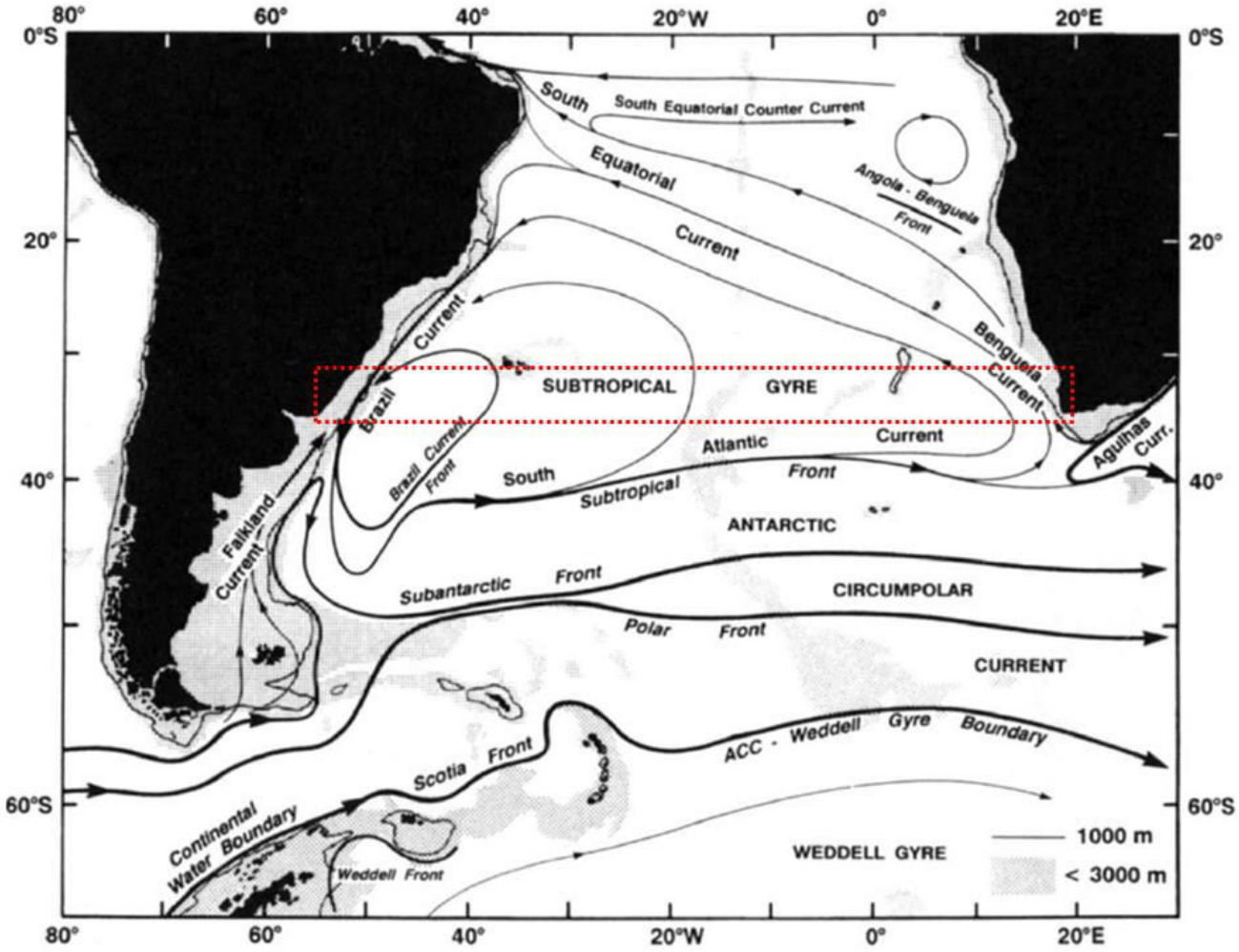

FIGURA 1: Representação esquemática da circulação de larga escala na camada superficial do oceano Atlântico Sul. O retângulo vermelho delimita a região de estudo do presente trabalho. Figura extraída e adaptada de Peterson & Stramma (1991).

O sistema de ressurgência da Corrente de Benguela é um dos mais produtivos do planeta, devido a células de ressurgência altamente produtivas que, no caso do sistema Benguela Sul são sazonais devido à variações na posição do centro de alta do oceano Atlântico Sul (Hutchings *et al.* 1995, 2009; Monteiro 2010). Devido a essa variação sazonal, as altas concentrações de fitoplâncton e mesozooplâncton estão em fase com o sistema de ressurgência, com picos no verão e no outono (Hutchington *et al.* 2009), originando taxas médias de produtividade entre 1.9 – 2.0 g C m^{-2} d^{-1} (ver Piontkovski *et al.* 2003).

O giro subtropical do Atlântico Sul apresenta limitação de nutrientes devido a uma nutriclina profunda, exceto durante a estação de inverno quando os ventos aumentam, aprofundando a camada de mistura e termoclina, permitindo a intrusão de nutrientes para profundidades mais rasas (Longhurst 1995). Essa maior disponibilidade de nutrientes favorece uma maior produtividade primária em seguida. Ainda, regiões ao longo da porção sul do giro são influenciadas pela migração sazonal da Frente Subtropical (ou Zona de Convergência Subtropical), localizada entre 35°S e 45°S (Peterson & Stramma 1991). Gonzalez-Silvera *et al.* (2004) demonstram essa

influência para a porção oceânica da frente desde a zona costeira sul-americana (~ 31°S até ~ 45°S) até cerca de 20°W. As correntes do giro, junto com a distribuição de temperatura, influenciam a distribuição de nutrientes e de fitoplâncton (Piontkovski *et al.* 2003). Essas influências, considerando a região do presente estudo, podem ocorrer da mistura de águas carregadas pela Corrente das Malvinas para a porção sudoeste do giro, oriunda de latitudes mais altas, e a Corrente de Benguela para a porção leste do giro, em que águas de camadas intermediárias ressurgem ricas em nutrientes (Hutchings *et al.*, 1995; Piola *et al.* 2000; Piontkovski *et al.* 2003).

1.3. MOTIVAÇÃO

Dentro do contexto de estudos de fluxos de CO_2 na interface oceano-atmosfera, o oceano Atlântico Sul é uma das regiões consideradas subamostradas (Takahashi *et al.* 2009) dos oceanos globais. Os trabalhos de CO_2 na interface oceano-atmosfera realizados até o presente momento focam-se em regiões específicas como a região tropical (Ternon *et al.* 2000, Lefèvre 2009, Koffi *et al.* 2010), porção austral (e.g. Chierici *et al.* 2004) e regiões costeiras (Ito *et al.* 2005, Bianchi *et al.* 2005, 2009, González-Dávila *et al.* 2009, Santana-Casiano *et al.* 2009). Estudos que abrangem o giro subtropical são poucos, representando, muitas vezes, apenas um hemisfério do giro – leste ou oeste ou já estão temporalmente defasados (Lefèvre *et al.* 2002, Padin *et al.* 2010), ou utilizam-se da interpolação, que muitas vezes geram dados espúrios, para compensar a falta de dados (Takahashi *et al.* 2002, 2009). Neste sentido, o presente trabalho contribui com dados sobre os fluxos líquidos de CO_2 ao longo de 35°S, propõe modelos preditivos da fCO_2 oceânica, em função de variáveis ambientais, bem como, colabora para a ampliação de bancos de dados da fCO_2 para futuros estudos.

OBJETIVOS

2. OBJETIVOS

2.1. OBJETIVO GERAL

Estimar os fluxos líquidos de CO_2 na interface oceano-atmosfera ao longo da latitude de 35°S do oceano Atlântico Sul e plataformas continentais adjacentes, visando determinar o comportamento da área de estudo como fonte ou sorvedouro de CO_2 da atmosfera e compreender a influência de processos físicos, químicos e biológicos nesta distribuição espacial.

2.2. OBJETIVOS ESPECÍFICOS

1. Determinar valores de fugacidade do CO_2 na atmosfera e na superfície oceânica e os fluxos líquidos de CO_2 entre o oceano e a atmosfera no Oceano Atlântico Sul, bem como, analisar as diferenças zonais desses valores ao longo da região de estudo;
2. Avaliar a influência de parâmetros bióticos (clorofila-a e oxigênio dissolvido) e abióticos (temperatura, salinidade) locais sobre os valores de fugacidade do CO_2 na superfície oceânica;
3. Modelar a fugacidade de CO_2 para a região de estudo a partir dos parâmetros de temperatura, salinidade e clorofila-a.

METODOLOGIA

3. METODOLOGIA

3.1. CONJUNTO DE DADOS

Os dados utilizados neste trabalho foram coletados, durante o período de 24 de outubro a 05 de dezembro de 2011 a bordo do NHo. Cruzeiro do Sul, da Marinha do Brasil (Figura 2). Amostrou-se a fração molar de CO_2 (xCO_2) na água do mar e na atmosfera com a utilização do sistema de medição contínua automático de pressão parcial de CO_2 (pCO_2) modelo 8050 (*General Oceanics Inc.)*. A amostragem de água do mar na coluna de água foi realizada com uso do sistema Roseta/CTD SBE 911+ acoplado a 12 garrafas de 5 litros em profundidades estabelecidas durante a descida do sistema Roseta/CTD. No total, 71 estações CTD foram ocupadas entre o Brasil e África.

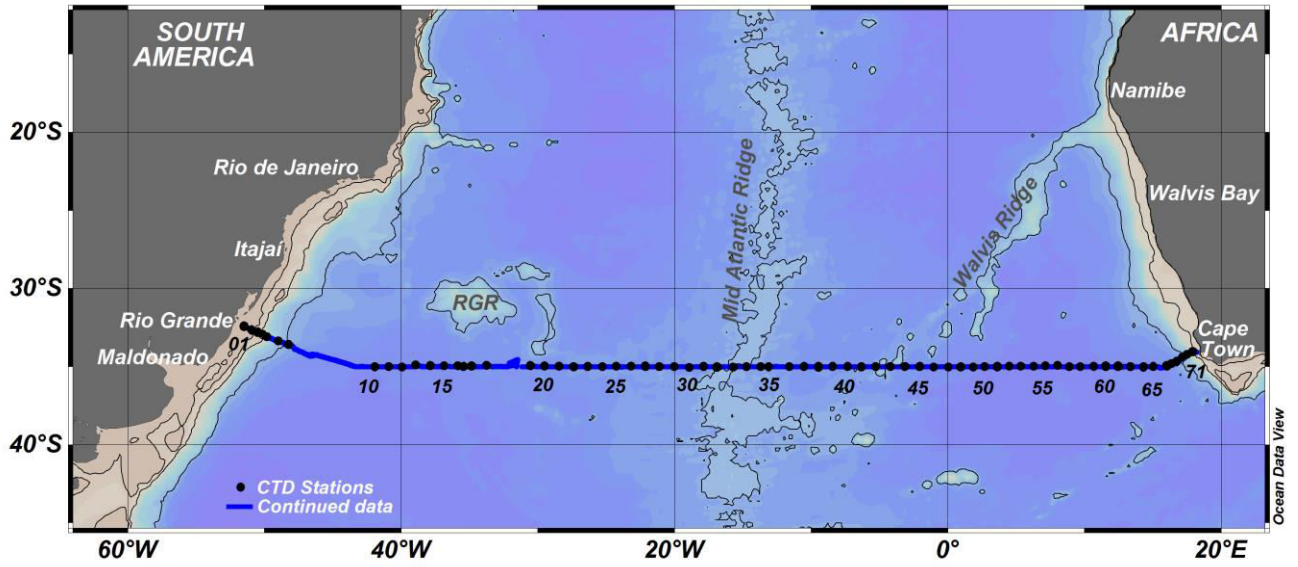

FIGURA 2: Área de estudo e rede de amostragem de água do mar durante as medições continuas de fração molar do CO_2 na superfície marinha e atmosfera, temperatura *in situ*, salinidade pratica e oxigênio dissolvido para o período do cruzeiro oceanográfico realizado entre 22 de outubro e 5 de dezembro de 2011, dentro do projeto "Medição e Modelagem de Fluxos de CO_2 no Atlântico Sul e Oceano Austral".

3.2. DETERMINAÇÃO DA FUGACIDADE E FLUXO LÍQUIDO DO CO_2

Para a medição de pressão parcial do CO_2 na superfície marinha, amostrou-se água do mar através de uma bomba submersível (a cerca de 6 m de profundidade) acoplada a uma tubulação que se conecta ao sistema equilibrador do instrumento de medição. Para amostragem do ar, conectou-se um tubo trançado ao equipamento, instalado na parte mais alta da embarcação, evitando-se a contaminação pela própria embarcação. A metodologia analítica de determinação da pCO_2 se baseia na amostragem contínua de água do mar a cada 80 segundos, com o sistema

automático da *General Oceanic Inc.* (modelo 8050) que consiste de duas fases: (1) uma célula de equilíbrio e (2) um analisador de CO_2/H_2O (LICOR 7000), com detecção infravermelha não dispersiva (Pierrot *et al.* 2009).

Este sistema funciona em modo de circuito fechado, em que a água do mar amostrada continuamente é injetada em um equilibrador sob a forma de um jato de *spray* que irá se equilibrar com o ar purgado do analisador. O volume de água dentro do equilibrador é constante devido a um dreno contido no mesmo, de modo que a coluna de ar é igual a 500 mL. A pressão é controlada pelo próprio equipamento, e a temperatura dentro do equilibrador, por um sensor de alta precisão. A mistura entre a água do mar e o ar ocorre em cerca de 4 minutos quando, então, o ar é bombeado (a cerca de 80 – 100 ml min^{-1}) por um sistema de tubos com condensador e dessecante que seca a amostra.

Para a amostra de ar, esta é amostrada e seca a 2 L de ar min^{-1}, sendo bombeado na mesma velocidade que a amostra de água do mar. Logo em seguida, as amostras entram no analisador infravermelho não dispersivo para medição das frações molares do CO_2 na água do mar ($x\mathrm{CO}_2^{\mathrm{mar}}$) e no ar ($x\mathrm{CO}_2^{\mathrm{ar}}$). Em ambas as medições, circulou-se continuamente ar seco livre de CO_2 na cela de referência do equipamento.

A cada 12 horas, o equipamento realizou calibração com quatro gases padrão com frações molares de CO_2 conhecidas. Além disso, entre os períodos de calibração, foram realizadas checagens a cada 3 horas com os mesmos gases para controle dos desvios de linha de base do equipamento. Os gases padrão utilizados para calibração eram da empresa White Martins, 'misturas padrão *master*', com concentrações de CO_2 de 255,2, 350,6, 390,0 e 473,2 ppm.

Para cada medição de $x\mathrm{CO}_2$, houve uma medição temperatura e salinidade *in situ* medidos de forma contínua pelo CTD Idronaut acoplado a este sistema. Ambos dados são utilizados nos cálculos das fugacidades do CO_2 no mar ($f\mathrm{CO}_2^{\mathrm{sw}}$) e no ar ($f\mathrm{CO}_2^{\mathrm{atm}}$) e fluxo líquido do CO_2 (FCO_2), realizados posteriormente.

3.2.1. Medição e correção dos dados de fração molar de CO_2

Para corrigir os desvios de linha de base do equipamento em relação à calibração, foram calculadas as variações entre os valores verdadeiros dos padrões (valor certificado dos padrões) e os valores medidos pelo aparelho, tanto no momento da calibração (valor da calibração), quanto após 3 horas de medição (valor da checagem). Para cada intervalo antecedente a uma checagem, determinou-se uma equação de correlação linear para cada padrão que determinava a derivação de seu comportamento durante o tempo de medição, num total de quatro equações. Após, cada uma dessas quatro equações foi aplicada em seu respectivo intervalo entre a leitura de calibração e a de checagem. Deste valor calculado, foram determinados os valores de cada padrão por hora de medição, sendo, então, novamente equacionados para obtenção do valor nominal dos padrões. A partir desses cálculos foram determinadas as equações de correção a serem aplicadas, a cada

intervalo entre checagens, aos dados de fração molar de CO2 medidos pelo equipamento (Pierrot *et al.* 2009).

3.2.2. Cálculo da fugacidade do CO_2 (fCO_2)

Com os dados de fração molar corrigidos, calculou-se, primeiramente, a pressão parcial de CO_2 da água, no sistema equilibrador, e da atmosfera (pCO_2^{eq}e pCO_2^{atm}, respectivamente) no momento da medição, segundo Takahashi *et al.* (2009), como demonstrado abaixo:

$$pCO_2^{eq} = xCO_2^{eq} \times [P_{baro}(eq) - P_o(eq)] \quad (1)$$

$$pCO_2^{atm} = xCO_2^{atm} \times [P_{baro}(ss) - P_o(ss)] \quad (2)$$

em que pCO_2^{eq} é a pressão parcial do CO_2 no equilibrador; xCO_2^{eq} é fração molar do CO_2 da água do mar (± 0,2) no equilibrador; xCO_2^{atm} é fração molar do CO_2 no ar (± 0,2); $P_{baro}(eq)$ é a pressão barométrica do gás no equilibrador; $P_{baro}(ss)$ é a pressão barométrica na superfície do mar; e P_o é a pressão de vapor da água no equilibrador ($P_o(eq)$) e na superfície do mar ($P_o(ss)$), calculado segundo Weiss & Price (1980).

As fugacidades do CO_2 para amostras atmosféricas (fCO_2^{atm}) e oceânicas (fCO_2^{sw}), foram calculadas a partir da correção de pCO_2^{atm} e pCO_2^{eq} para o comportamento não ideal do CO_2, segundo Weiss (1974), descritas nas equações 3 e 4:

$$fCO_2^{atm} = pCO_2^{atm} \times \exp\left[\frac{-1636{,}75+12{,}0408.SST-0{,}0327957.SST^2+0{,}0000316528.SST^3+2.(57{,}7-0{,}118.SST)}{82{,}0578.SST}\right] \quad (3)$$

$$fCO_2^{eq} = pCO_2^{eq} \times \exp\left[\frac{-1636{,}75+12{,}0408.T_{eq}-0{,}0327957.{T_{eq}}^2+0{,}0000316528.{T_{eq}}^3+2.(57{,}7-0{,}118.T_{eq})}{82{,}0578.T_{eq}}\right] \quad (4)$$

em que SST (± 0,01) é a temperatura da amostra *in situ* e T_{eq} (± 0,01) é a temperatura da amostra durante o equilíbrio.

Depois de calculados, os dados de fCO_2^{eq} foram corrigidos para os valores de SST, chegando-se à fugacidade do CO_2 na água do mar propriamente dita (fCO_2^{sw}), utilizando-se a equação empírica (5) proposta por Takahashi *et al.* (2009):

$$fCO_2^{sw} = fCO_2^{eq} \times \exp\left[(SST - T_{eq}) \cdot 0{,}0423\right] - 4{,}35 \times 10^{-5}(SST^2 - T_{eq}^2) \quad (5)$$

em que, fCO_2^{sw} é a fugacidade do CO_2 corrigida para a temperatura *in situ*, fCO_2^{eq} é a fugacidade do CO_2 à temperatura da amostra no equilibrador.

3.2.3. Cálculo da fugacidade normalizada

Normalizou-se os dados de fCO_2^{sw} para a temperatura média do cruzeiro, de 16,41 °C, de acordo com a equação 6 (Takahashi *et al.* 2009), a fim de avaliar o efeito da temperatura nas distribuições da fCO_2^{sw}.

$$fCO_{2-N16.41}^{sw} = fCO_2^{sw} \times \exp\{0{,}0433(\overline{T} - T_{is}) - 4.35 \cdot 10^{-5}[\overline{T}^2 - T_{is}^2]\} \quad (6)$$

em que $\bar{T}$ é a temperatura média do cruzeiro.

3.2.4. Cálculo do fluxo líquido de CO_2

O fluxo líquido de CO_2 na interface mar-ar pode ser calculado através da expressão:

$$FCO_2 = k.K_o.\Delta fCO_2 \quad (7)$$

em que, k é o coeficiente da velocidade de transferência do CO_2, K_o é o coeficiente de solubilidade do CO_2 na água do mar (Weiss 1974) e ΔfCO_2 é a diferença entre fCO_2^{sw} e fCO_2^{atm}.

O coeficiente da velocidade de transferência de um gás depende da velocidade do vento e do Número de Schmidt que representa a razão entre a taxa de difusão viscosa e a taxa de difusão molecular do gás (Weiss 1984; Liss & Merlivat 1986). Utilizou-se dados de médias mensais (outubro, novembro e dezembro de 2011) das componentes u e v da velocidade do vento, extraídas do banco de dados do NCEP_Reanalysis 2 fornecidos por NOAA/OAR/ESRL PSD, Boulder, Colorado, USA, a partir do site http://www.esrl.noaa.gov/psd/ (Kanamitsu *et al.*, 2002).

Os coeficientes da velocidade de transferência calculados variam conforme o autor, sendo que para este estudo foram calculados os coeficientes de transferência do gás CO_2 referentes a 3 autores: Wanninkhof (1992), Nightingale *et al.* (2000), e Takahashi *et al.* (2009). As respectivas equações para cálculo de k estão resumidas na TABELA 1. Os fluxos calculados serão referidos a partir de agora de acordo com seu autor, ou seja, W92, N00 e T09, respectivamente.

TABELA 1: Valores de coeficientes de transferência calculados, sendo que u é a velocidade do vento em m s-1 a 10 m acima do nível do mar e Sc é o número de Schmidt.

Autor	k
Wanninkhof (1992)	$k = 0{,}39\,u^2 \cdot \left(660/_{Sc}\right)^{-1/2}$
Nightingale *et al.* (2000)	$k = [0{,}222u^2 + 0{,}1\,u] \cdot \left(600/_{Sc}\right)^{-1/2}$
Takahashi *et al.* (2009)	$k = 0{,}26\,u^2 \cdot \left(660/_{Sc}\right)^{-1/2}$

3.3. DADOS COMPLEMENTARES

3.3.1. Oxigênio dissolvido e saturação do oxigênio

Medidas de oxigênio dissolvido foram realizadas durante o cruzeiro de três formas distintas: (1) método de Winkler modificado (Culberson 1991), utilizado em amostras de água do mar coletadas durante a derrota do cruzeiro, para todas as estações oceanográficas realizadas; (2) CTD principal do cruzeiro, CTD SBE 911+; e (3) CTD Idronaut, pertencente ao sistema de medição de CO_2, com sensor polarográfico com cátodo de platina-iridium e ânodo de prata (precisão de 99,99%). Os valores medidos pelos CTDs foram calibrados com base nos valores de oxigênio dissolvido medidos pelo método de Winkler modificado.

3.3.2. Clorofila-a total *in-situ*

Neste estudo, os valores de clorofila-a foram utilizados como um indicador de biomassa fitoplanctônica. A concentração total (monovinyl + divinyl) de clorofila-*a* foi determinada utilizando a metodologia de HPLC (*High Performance Liquid Chromatography* - Cromatografia Líquida de Elevada Precisão). Os dados de concentração total de clorofila-a foram processados e cedidos pelo Dr. Carlos Rafael Mendes do Laboratório de Ecologia de Fitoplâncton e Microorganismos Marinhos do Instituto de Oceanografia da Universidade Federal do Rio Grande, sob reponsabilidade da Profª. Dra. Virgínia Maria Tavano.

3.4. MODELOS DE PREVISÃO DA FUGACIDADE DO CO_2

3.4.1. MODELO POR REGRESSÃO LINEAR MÚLTIPLA

Modelos de regressão linear múltipla (MRL) baseiam-se na teoria da regressão linear em que a variável resposta apresenta relação linear com as variáveis preditivas. Assim, através dessa metodologia, calcula-se os coeficientes referentes às correlações lineares entre as variáveis preditivas e a variável resposta, além de um valor intercepto. A partir desses coeficientes, monta-se a equação preditiva para a variável resposta (Neter *et al.* 1983, Triola 2008). Modelos de previsão de CO_2 utilizam basicamente como variáveis preditivas, a temperatura, a salinidade e a concentração de clorofila-a (Lefèvre & Taylor 2002, Chierici *et al.* 2009, Padin *et al.* 2010; Hales *et al.* 2012). Neste trabalho, utilizou-se o modelo MRL a fim de estabelecer uma equação para cálculo de fCO_2 na água do mar na região do presente estudo. Utilizou-se o software MATLAB 7.10.0 R2010a para os cálculos, sendo que a equação a ser estabelecida é descrita abaixo:

$$fCO_{2-\mathrm{MRL}} = \alpha + (\beta_1 \cdot \mathrm{CSAT}) + (\beta_2 \cdot \mathrm{SST}) + (\beta_3 \cdot \mathrm{SSS}) \qquad (8)$$

sendo que α é o intercepto da reta de regressão linear e β_i são os parâmetros desconhecidos a serem determinados nesta análise. SST e SSS são a temperatura e a salinidade *in situ* respectivamente, enquanto CSAT é a concentração de clorofila-a extraída de imagens de satélite.

Extração dos dados de concentração de clorofila-a de imagens de satélites

Utilizou-se dados de concentração de clorofila-a estimadas por sensores a bordo de satélites como uma das variáveis preditivas do modelo MRL, pois fornecem maior resolução espacial do que os dados das estações de CTD. Imagens de satélite diárias da concentração de clorofila-a total, de 4 km de resolução, para todo o período do cruzeiro foram obtidas do sensor MODIS-AQUA, através do *Ocean Color Group* da NASA (http://oceancolor.gsfc.nasa.gov/). Foi extraído o valor da concentração de clorofila-a para cada dia respectivo de cruzeiro. Quando havia cobertura de nuvens no local da medição de fCO_2^{sw}, utilizou-se a média daquele dia ± 1 dia. No caso de persistência de nuvens, utilizou-se a média da concentração de clorofila-a do dia ± 2 dias. Se ainda persistia nuvem (ou ausência de dado) naquela posição geográfica, o valor da clorofila-a permanecia desconhecido. Como os dados de clorofila-a estão distribuídos em uma grade de 4 x 4 km, os dados de temperatura e salinidade, obtidos continuamente pelo CTD Idranaut, também foram ajustados para uma grade de mesma resolução.

3.4.2. MODELO LINEAR GENERALIZADO

Desenvolvido por John Nelder e R.W.M. Wedderburn em 1972, o Modelo Linear Generalizado, ou GLM (*Generalized Linear Model - GLM*), como é comumente conhecido, é uma síntese e extensão do modelo de regressão linear simples. O GLM permite obter uma variável resposta que tem uma distribuição diferente da normal ou gaussiana, pois generaliza a regressão linear ao permitir que a variável resposta seja relacionada com as variáveis preditivas através de uma função de ligação e permitindo que a magnitude da variância de cada medição também seja função de seu valor previsor (Faraway 2006, Zuur *et al.* 2009). Visto que em estudos oceanográficos trabalha-se com alta variabilidade de dados que podem não apresentar distribuição normal, a aplicação do GLM pode ser um modelo melhor aplicado para esse tipo de dados. Dessa forma, utilizou-se o GLM para inferir uma equação de previsão de fCO_2 para a região de estudo, sendo que a equação resultante segue o seguinte padrão:

$$fCO_{2-\mathrm{GLM}} = \gamma + (\delta_1 \cdot \mathrm{CSAT}) + (\delta_2 \cdot \mathrm{SST}) + (\delta_3 \cdot \mathrm{SSS}) \qquad (9)$$

em que γ é o intercepto da reta de regressão linear e δ_i são os parâmetros desconhecidos a serem determinados para cada variável preditiva nesta análise; SST, SSS e CSAT são os mesmo dados de temperatura, salinidade e concentração de clorofila-a utilizados para o modelo MRL descrito acima.

MANUSCRITO

SEA-AIR CARBON DIOXIDE FLUXES ALONG 35˚S LATITUDE IN THE SOUTH ATLANTIC OCEAN AND ADJACENT CONTINENTAL SHELVES

ABSTRACT

Average atmospheric CO_2 reached levels above 400 ppm during 2014. The oceans play an important role in absorbing a significant fraction of the atmospheric CO_2 surplus, but there are uncertainties concerning several oceanic regions, such as the under-sampled South Atlantic Ocean. This study assessed the net sea-air CO_2 fluxes along the 35°S latitude and adjacent continental shelves during 2011 spring and early summer periods. Underway CO_2 molar fraction, temperature, salinity and dissolved oxygen measurements were taken continuously from Brazil to Africa. Values of both satellite and discrete *in-situ* chlorophyll-a concentration along the ship's track were used as support data. The sea-surface CO_2 fugacity in (fCO_2^{sw}) and difference in sea-air fugacity (ΔfCO_2^{sw}) showed high variability along the cruise track, with higher values found on the continental shelf and slope regions. All ΔfCO_2^{sw} values were negative, meaning that a sinking process was occurring during the cruise period, yielding an average net CO_2 flux of -3.1 ± 2.2 mmol m^{-2} day^{-1} (using Wanninkhof 1992). Surface temperature and salinity were the main drivers of fCO_2^{sw} variability and chlorophyll-a showed little relation to CO_2 data in the whole area. Algorithms for fCO_2 and normalized fCO_2 were developed for the South American coastal, oceanic and African regions. Normalized fCO_2 models presented better results, especially in the western portion (Brazil coast to 20° W) of the study area.

KEY WORDS

CO_2 fugacity, Subtropical South Atlantic Ocean, continental shelf, sea-air CO_2 flux

1. Introduction

Atmospheric CO_2 concentrations have reached levels higher than any estimated values in the last 800.000 years (Luthi *et al.* 2008; IPCC 2013). Monthly levels above 400 ppm were recorded for several months in 2014 (Tans & Keeling 2014), which are much higher than the pre-industrial 280 ppm. In addition, the last IPCC Report (2013) confirmed that human activities are an influencing factor over climate change due to fossil fuel burning, cement production and land-use changes. Based on studies of CO_2 global budget, it is estimated that the oceans absorbed 2.6 ± 0.5 Gt C y^{-1} in the 2003-2012 period (Le Quéré *et al.* 2013). Therefore, studies which elucidate CO_2 absorption and/or release processes in the oceans are vitally important to understand the global carbon cycle.

In the last climatological global evaluation of sea-air CO_2 fluxes, Takahashi *et al.* 2009 estimated that oceans absorbed 2.0 ± 1.0 Pg C yr^{-1} for the base year 2000. Temperate ocean regions were considered the largest sink for atmospheric CO_2, where about -0.70 Pg C yr^{-1} was attributed to the northern, and -1.05 Pg C yr^{-1}, to the southern hemisphere, respectively. However, a relatively low progress has been made on CO_2 flux studies in the Southern Hemisphere. Continental shelves have received special attention in recent years (Bozec *et al.* 2005, Ito *et al.* 2005, Jiang *et al.* 2008, Bianchi *et al.* 2005, 2009, Lefèvre 2009, Santana-Casiano *et al.* 2009), which allowed to infer that coastal regions can be either sources or sinks of CO_2, depending on the dynamics and constraints of each region (Borges *et al.* 2005, Chen & Borges 2009).

Tsunogai *et al.* (1999) introduced the concept of c*ontinental shelf pump* which would be responsible for 1 Gt C yr^{-1} if all coastal zones had the same absorption rate as the East China Sea. Borges (2005) considered the global coastal ocean as CO_2 sinking zones (-1.17 mol C m^{-2} yr^{-1}) when estuarine and salt marshes were not included, and as small CO_2 sources (0.38 mol C m^{-2} yr^{-1}) when these were added. By using a larger and more heterogeneous dataset, Cai *et al.* (2006) showed that low latitude shelves were also considered CO_2 sources to the atmosphere (0.11 Pg C yr^{-1}), while shelves at mid-high latitudes acted as CO_2 sinks (-0.33 Pg C yr^{-1}). In another study, the coastal data was divided into two categories, where continental shelves acted as sinking zones (-0.33 a -0.36 Pg C yr^{-1}), whereas nearshore ecosystems acted as source zones (0.50 Pg C yr^{-1}) (Chen & Borges, 2009). Moreover, it was estimated that the southwestern South Atlantic were a sink region (-1.0 mol CO_2 m^{-2} yr^{-1}) and the southeastern boundary were CO_2 source zone (0.5 mol CO_2 m^{-1} yr^{-1}). On the other hand, Laruelle *et al.* (2010) found that temperate upwelling systems of the Atlantic Ocean are a net sink for atmospheric CO_2 (-1.6 ± 1.0 mol C m^{-2} yr^{-1}), contrasting with positive net carbon fluxes in the Pacífic and Indian Oceans (3.2 ± 2.4 e 0.9 ± 1.2 mol C m^{-2} yr^{-1}, respectively), and that estuarine regions sea-air CO_2 flux are estimated 28.5 ± 15.8 mol C m^{-2} yr^{-1}.

Coastal zones are highly dynamic environments, in terms of both physical and biological processes, due to proximity to the continent (Garcia & Garcia 2008). Therefore, several processes

may regulate net sea-air CO_2 fluxes as well the CO_2 export at those areas (Borges *et al.* 2005). Despite their importance, coastal zones are still under-sampled for CO_2 fluxes and, therefore, they are not adequately represented by current CO_2 models, nor are properly considered at global estimates (Orr *et al.* 2001; Sarmiento & Gruber 2002; Takahashi *et al.* 2009).

In this present work, we present the sea-air CO_2 fluxes as well as the behavior of seawater CO_2 fugacity along the latitude of 35°S in the South Atlentic Ocean and two dynamic different continental shelves (South America and African shelves). We explain the principal factors controlling seawater CO_2 fugacity, and consequently, the sea-air CO_2 fluxes. Also we contribute to a better comprehension of the oceanic CO_2 system.

Study area

The southern portion of the South Atlantic subtropical gyre referred in this study comprises an oceanic region along the 35˚S line from South American to African continental shelves. The main general circulation features (Figure 1) in the study region include Brazil Current (BC), a western boundary current that flows southward, eastward South Atlantic Current (SAC) and Benguela Current (BgC), an eastern boundary current (Peterson & Stramma 1991).

The western shelf is a highly dynamic area, with sazonal and interannual variability, due to influence of Plata Plume Water (PPW) and Patos Lagoon Water (PLW). PPW can reach Santa Marta's Cape (approximately 28ºS) in winter, while it is restricted to shelf waters adjacent to the river mouth during summer periods (Möller *et al.* 2008). In the open ocean, SAC is formed from the eastern flow generated by the Brazil-Malvinas Confluence at 38˚S. This current flows meandering towards the African continent where it contributes to the formation of the Benguela Current system (Stramma & England 1999). Concerning biological productivity, the Uruguayan and Southern Brazilian continental shelves are highly productive regions, by nutrient input from La Plata river discharge and, to a lesser extent, by the Patos Lagoon plume (Muelbert *et al.* 2008). Interaction between different shelf waters as well as input from South Atlantic Central Water (SACW), due to mesoscale events, also introduce nutrients into the shelf (Piola *et al.* 2000; Gonzalez-Silvera *et al.* 2008; Muelbert et al 2008). Primary productivity can reach approximately 160 gC m^{-2} yr^{-1} (see Muelbert *et al.* 2008).

The eastern shelf (adjacent to South Africa) comprises the southern section of Benguela Current Large Marine Ecosystem (BCLME), one of the four most important upwelling ecosystems in global eastern boundaries (Monteiro 2010). At surface, the current flows equatorward, generating intense upwelling cells between 15˚S - 37˚S, such as Cape Columbine Cell (33˚S) and Cape Peninsula Cell (34˚S). The southernmost zone of the BCLME presents seasonal upwelling during austral spring and summer (Shillington *et al.* 2006, Monteiro 2010). In this region, the Benguela upwelling system is one of the most productive regions on the planet, as consequence of those nutrient-rich upwelling cells (Hutchings *et al.* 2009; Gregon *et al.* 2013). The upwelling system is

subject to seasonal variation, due to displacement in the pressure center of the South Atlantic (Hutchings *et al.* 2009; Monteiro 2010). This produces important impacts on phytoplankton and mesozooplankton, which peaks in summer and autumn, with mean productivity rates ranging from 1.9 to 2.0 gC m^{-2} d^{-1} (see Piontkovski *et al.* 2003; Hutchington *et al.* 2009). Furthermore, anti-cyclonic eddies generated by the Agulha's retroflection zone are usually present in the adjacent oceanic region (Gordon *et al.* 1987).

The South Atlantic subtropical gyre is nutrient-limited due to stratification and a deep nutricline, except during the winter season, when wind speed increases and the mixing layer is deepened, breaking the thermocline and injecting nutrients to the surface layers, favoring primary productivity (Longhurst 1995). The southernmost section of the gyre is influenced by seasonal migration of the Subtropical Front, which brings relatively richer waters from higher latitudes that mix with oligotrophic gyre waters. (Peterson & Stramma 1991; Gonzalez-Silvera *et al.* 2004). This has been shown to be particularly important in the southwestern oceanic portion of the gyre (from ~ 31°S to ~ 45°S) from the outer shelf up to 20°W (Gonzalez-Silvera *et al.* 2004). Likewise, the currents system that forms the subtropical gyre affects nutrient and phytoplankton distribution (Piontkovski *et al.* 2003).

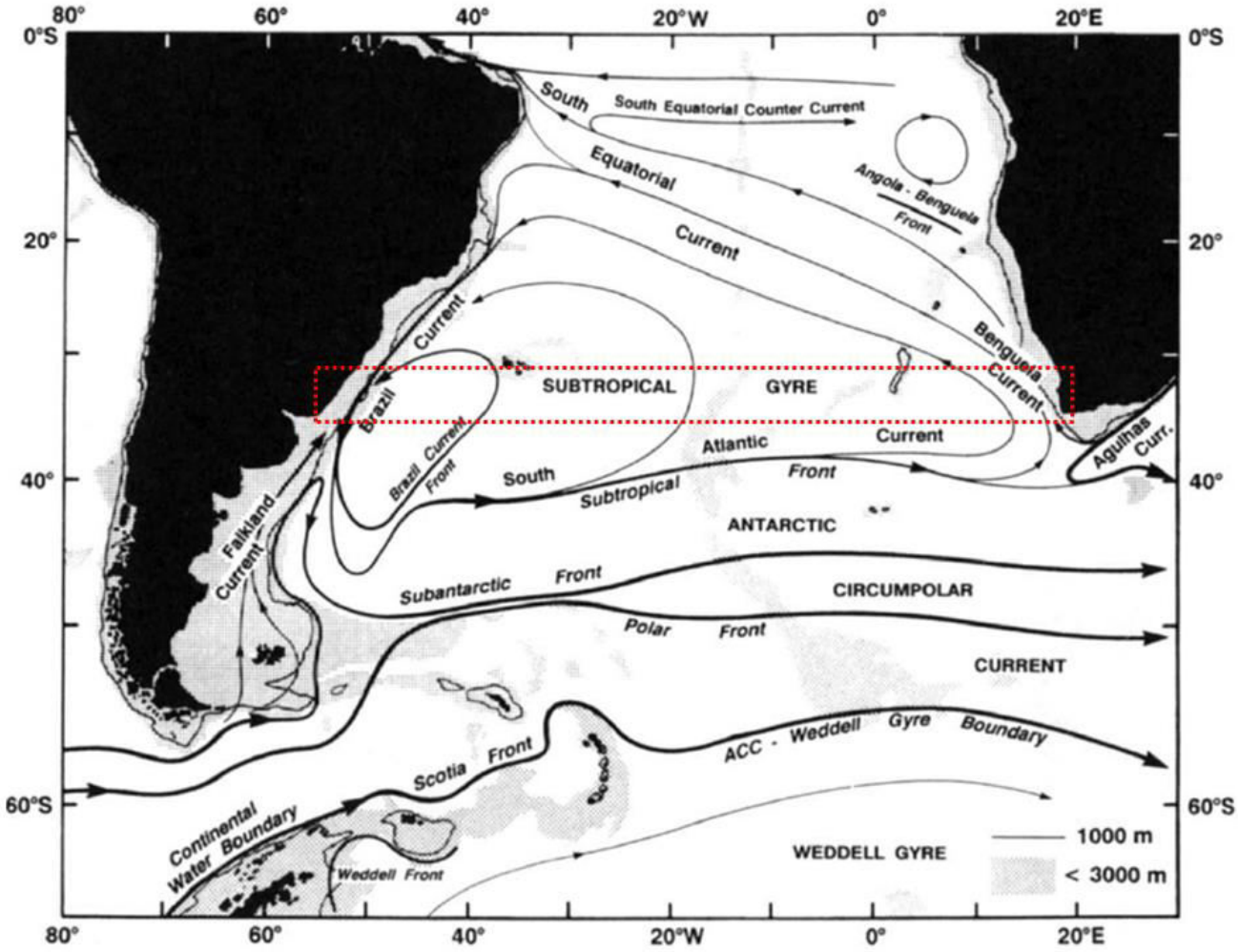

FIGURE 1 – Representation of surface general circulation of the South Atlantic Ocean. The red rectangle encloses the study area. Figure extracted and adapted from Peterson & Stramma (1991).

The study area in this work comprises three major ocenaographic systems: Brazil-Malvinas Confluence Zone in the southwestern section, South Atlantic Current, and Benguela Current, including its upwelling filaments in the southeastern domain. Those regions of the South Atlantic Ocean are mostly under-sampled, in terms of pCO_2 studies (Takahashi *et al.* 2009), as compared to the tropics (e.g. Ternon *et al.* 2000, Lefèvre 2009, Koffi *et al.* 2010), the austral section (e.g. Chierici *et al.* 2004) and coastal areas (e.g. Ito *et al.* 2005, Bianchi *et al.* 2005, 2009, González-Dávila *et al.* 2009, Santana-Casiano *et al.* 2009). Lack of studies on CO_2 fluxes in the subtropical gyre has been previously pointed out (Robinson *et al.* 2006; Takahashi *et al.* 2009). The present work aims to contribute with data on longitudinal distribution of net sea-air CO_2 fluxes along 35˚S in the South Atlantic Ocean and adjacent shelves, helping understand the status of the region either as sink or source of atmospheric CO_2.

2. Data and Methods

2.1 Data set

Data in this work was collected between October 24 and December 05, 2011 on board the Brazilian R.V. *Cruzeiro do Sul*. Underway surface seawater and atmospheric CO_2 molar fraction (xCO_2^{sw} and xCO_2^{air} respectively) data were taken along the ship track between Brazil and Africa (Figure 2). Continuous temperature, salinity and dissolved oxygen (by a polarographic sensor with platinum-iridium cathode and silver anode) data were sampled by an Idronaut CTD system. During the cruise, 71 CTD stations were occupied and seawater was sampled from several depths by a Carrousel/CTD SBE 911+ with 12 5-liter bottles.

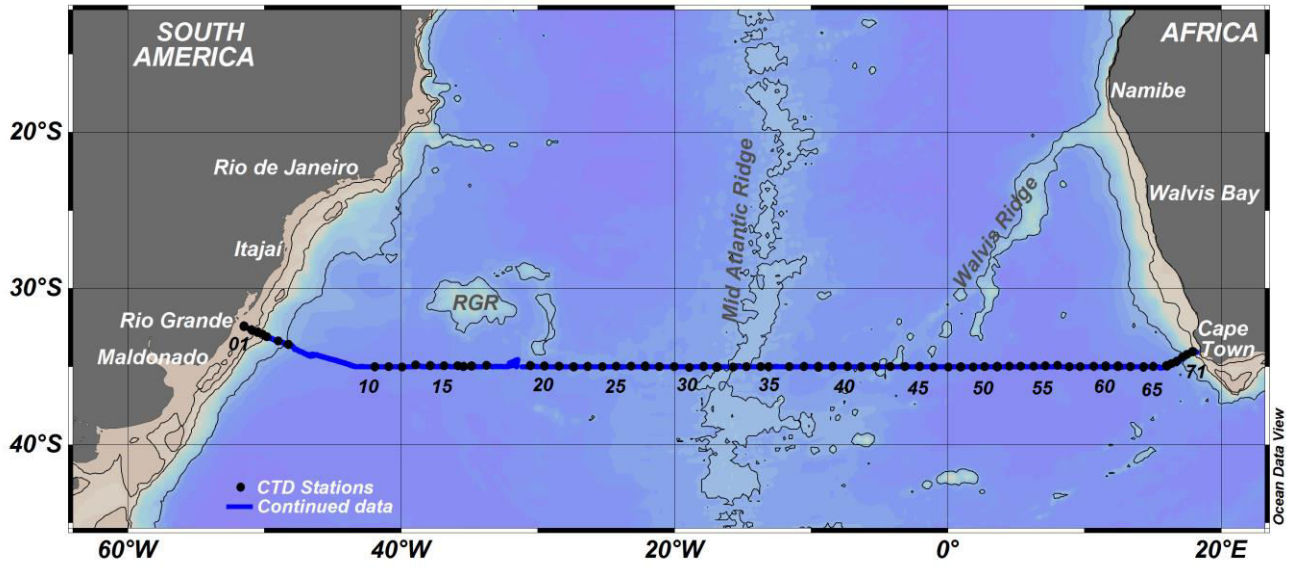

FIGURE 2 – Study region, ship track continuous measurements of CO_2 molar fraction in seawater and the atmosphere (blue line), and CTD stations (black dots) from October 22 to December 5, 2011. The cruise is part of the project 'Measurements and Modeling of CO_2 fluxes in the South Atlantic and Austral oceans".

2.2 Carbon dioxide fugacity determination (*f*CO_2)

Both seawater and air molar fractions were determined by an autonomous underway pCO_2-measuring system (General Oceanics Inc., 8050 model) that consisted of basically two phases: (1) an equilibrating cell, and (2) a CO_2/H_2O analyzer (LI-COR 7000) with a non-dispersive infrared detector. The pressure in the equilibrating cell is in constant ambient pressure due to a second smaller equilibrator that is connected to it, which replaces any gas lost from the main equilibrating cell. The temperature in the equilibrator is closely monitor, being measured by a very accurate (± 0.01 °C) Hart® digital thermometer with a thermistor probe (Pierrot *et al.* 2009).

The continuous measurements were made every 80 seconds, with a system calibration every 13 hours. Between calibrations a sequence of CO_2 standard gases (every three hours), atmospheric (every 1 ½ hour) and seawater (every 1 ½ hour) samples were made and repeated

four times in average during this interval. The seawater was pumped from a 6 m depth, while the air samples were pumped from the top of the vessel to avoid possible ship contamination. In both measurements, the analyzer is calibrated using four CO_2 standard gases (White Martins) with known molar fractions of 255.2, 350.6, 390.0 and 473.2 ppm. The respective continuous xCO_2, temperature, and salinity measurements were used to compute pCO_2^{eq} and pCO_2^{atm}, following Takahashi *et al.* (2009) equations:

$$pCO_2^{atm} = xCO_2^{atm} \times [P_{baro}(ss) - P_o(ss)] \qquad (1)$$

$$pCO_2^{eq} = xCO_2^{eq} \times [P_{baro}(eq) - P_o(eq)] \qquad (2)$$

In the equations above, pCO_2^{atm} and pCO_2^{eq} are, respectively, the CO_2 partial pressure in air and seawater in the equilibrium cell; $P_{baro}(ss)$ and $P_{baro}(eq)$ are barometric pressures at sea surface and in the equilibrating cell respectively; and, $P_o(ss)$ and $P_o(eq)$ are water vapor pressures at sea surface and in the equilibrating cell (Weiss & Price 1980) respectively.

The CO_2 fugacity for oceanic surface water (fCO_2^{sw}) and atmosphere (fCO_2^{atm}) were then calculated from partial pressure corrected for CO_2 non-ideal behavior using Weiss (1974) equation described below:

$$fCO_2^{atm} = pCO_2^{atm} \times \exp\left[\frac{-1636{,}75 + 12{,}0408.SST - 0{,}0327957.SST^2 + 0{,}0000316528.SST^3 + 2.(57{,}7 - 0{,}118.SST)}{82{,}0578.SST}\right] \quad (3)$$

$$fCO_2^{eq} = pCO_2^{eq} \times \exp\left[\frac{-1636{,}75 + 12{,}0408.T_{eq} - 0{,}0327957.{T_{eq}}^2 + 0{,}0000316528.{T_{eq}}^3 + 2.(57{,}7 - 0{,}118.T_{eq})}{82{,}0578.T_{eq}}\right] \quad (4)$$

where fCO_2^{atm} is CO_2 fugacity in atmosphere (± 0.1), fCO_2^{eq} is CO_2 fugacity in the equilibrating cell, SST is sea surface temperature (± 0.01) and T_{eq} is sample's temperature (± 0.01) during equilibrium.

The fCO_2^{sw} was then corrected for the difference between the equilibrator and *in-situ* temperatures following Takahashi *et al.* (2009):

$$fCO_2^{sw} = fCO_2^{eq} \times \exp\left[(SST - T_{eq}) \cdot 0{,}0423\right] - 4{,}35 \cdot 10^{-5}(SST^2 - T_{eq}^2) \qquad (5)$$

2.3 Net sea-air carbon dioxide flux determination (FCO_2)

Net sea–air CO_2 flux (FCO_2) for CO_2 fugacity was calculated using the expression:

$$FCO_2 = k.K_o.\Delta fCO_2 \qquad (6)$$

where k is CO_2 gas transfer velocity coefficient, K_o is CO_2 gas solubility coefficient (Weiss 1974), and ΔfCO_2 is the difference between fCO_2^{sw} and fCO_2^{atm}.

The CO_2 gas transfer velocity coefficients (Table 1) were estimated using the formula in Wanninkhof (1992), Nightingale *et al.* (2000), and Takahashi *et al.* (2009), hereinafter W92, N00, and T09 respectively and were used to compare with previous works. For calculation of k, monthly mean wind speed data was used from NCEP-DOE AMIP-II Reanalysis data provided by NOAA/OAR/ESRL PSD, Boulder, Colorado, USA, from *http://www.esrl.noaa.gov/psd/* (Kanamitsu *et al.*, 2002).

TABLE 1: CO_2 gas transfer velocity coefficient used with wind speed (u, m s^{-1}) at 10 m above sea level and Sc as Schmidt number.

Autor	k
Wanninkhof (1992)	$k = 0{,}39\, u^2 \cdot \left({}^{660}/_{Sc}\right)^{-1/2}$
Nightingale *et al.* (2000)	$k = [0{,}222u^2 + 0{,}1\, u] \cdot \left({}^{600}/_{Sc}\right)^{-1/2}$
Takahashi *et al.* (2009)	$k = 0{,}26\, u^2 \cdot \left({}^{660}/_{Sc}\right)^{-1/2}$

2.4 Dissolved oxygen and chlorophyll-a

Continuous dissolved oxygen (DO) measurements obtained by an Idronaut oxygen sensor with platinum-iridium cathode and silver anode. This data was adequately corrected for the dissolved oxygen values from the OD measurements by the modified Winkler's method (Culberson 1991).

In-situ chlorophyll-a data was used in this work as an index of phytoplankton biomass in the regions where chlorophyll-a satellite data was no available. Surface water samples for chlorophyll-a determination were filtered on Whatman GF/F and filters were immediately frozen in liquid nitrogen. In the laboratory, the pigment extraction was made with methanol (95% buffered with 2% ammonium acetate). After adequate extraction procedures, chlorophyll-a concentration was determined in a Shimatzu HPLC (Zapata *et al.* 2000; Mendes *et al.* 2007).

2.5 Prediction model for fCO_2

2.5.1 Multiple Linear Regression Model (MLR model)

A multiple linear regression model was used to predict fCO_2 in the study region, based on observed sea surface temperature (SST), sea surface salinity (SSS) and satellite-derived chlorophyll-a concentration (CSAT) data. SST and SSS were continuously measured (every 80 seconds) during the cruise by the Idronaut CDT while CSAT was retrieved from daily MODIS-AQUA satellite images. The MLR model equation is given by:

$$fCO_{2-MRL} = \alpha + (\beta_1 \cdot CSAT) + (\beta_2 \cdot SST) + (\beta_3 \cdot SSS) \qquad (7)$$

where α is the intercept of the linear regression, and β_i are the unknown coefficients to be determined for each parameter.

Extraction of chlorophyll concentration from satellite images

Chlorophyll concentration (CSAT) was extracted from daily MODIS-AQUA satellite images (4 km) for the entire cruise period from (http://oceancolor.gsfc.nasa.gov/). One CSAT value was extracted for each cruise day, coinciding with fCO_2^{sw} measurements positions. On cloudy days, average CSAT values were retrieved for that day ± 1 day or ± 2 days, when cloudiness persisted, on a geographical position. Continuous SST and SSS data were adjusted to CSAT grid resolution (4 x 4 km).

3. Results

3.1 Characterization of the study area

Figure 3a shows potential temperature-salinity (θ-S) diagram for surface waters (6 metros) where water masses were identified according to indices in the literature (see Table 2). Three main sub-regions were identified from this diagram: (1) continental shelf and adjacent oceanic area in the South American sub-region (Fig. 3b) where Plata Plume Water (PPW), Tropical Water (TW), Subtropical Shelf Water (STSW) and South Atlantic Central Water (SACW) are present; (2) oceanic sub-region with presence of SACW (Figure 3c) and modified Subtropical Surface Water (mSTSW); and (3) African sub-region with modified Subtropical Surface Water (mSTSW) and SACW (Fig. 3d).

TABLE 2: T-S indices used for identification of water masses at each sub-region in the study area, with corresponding reference.

Water Mass	Temperature (°C)	Salinity	Author
Plata Plume Water (PPW)	T > 10	S ≤ 33.5	
Subtropical Shelf Water (STSW)	14 < T < 21	33.5 < S < 36	Summer indexes from Möller *et al.* (2008)
Tropical Water (TW)	T ≥ 18.5	S ≥ 36	
South Atlantic Central Water (SACW)	T ≤ 18.5	S ≥ 34.3	Stramma & England (1999)
Modified Subtropical Surface Water (mSTSW)	T > 16	35.3 < S < 35.7	Gordon *et al.* (1987)

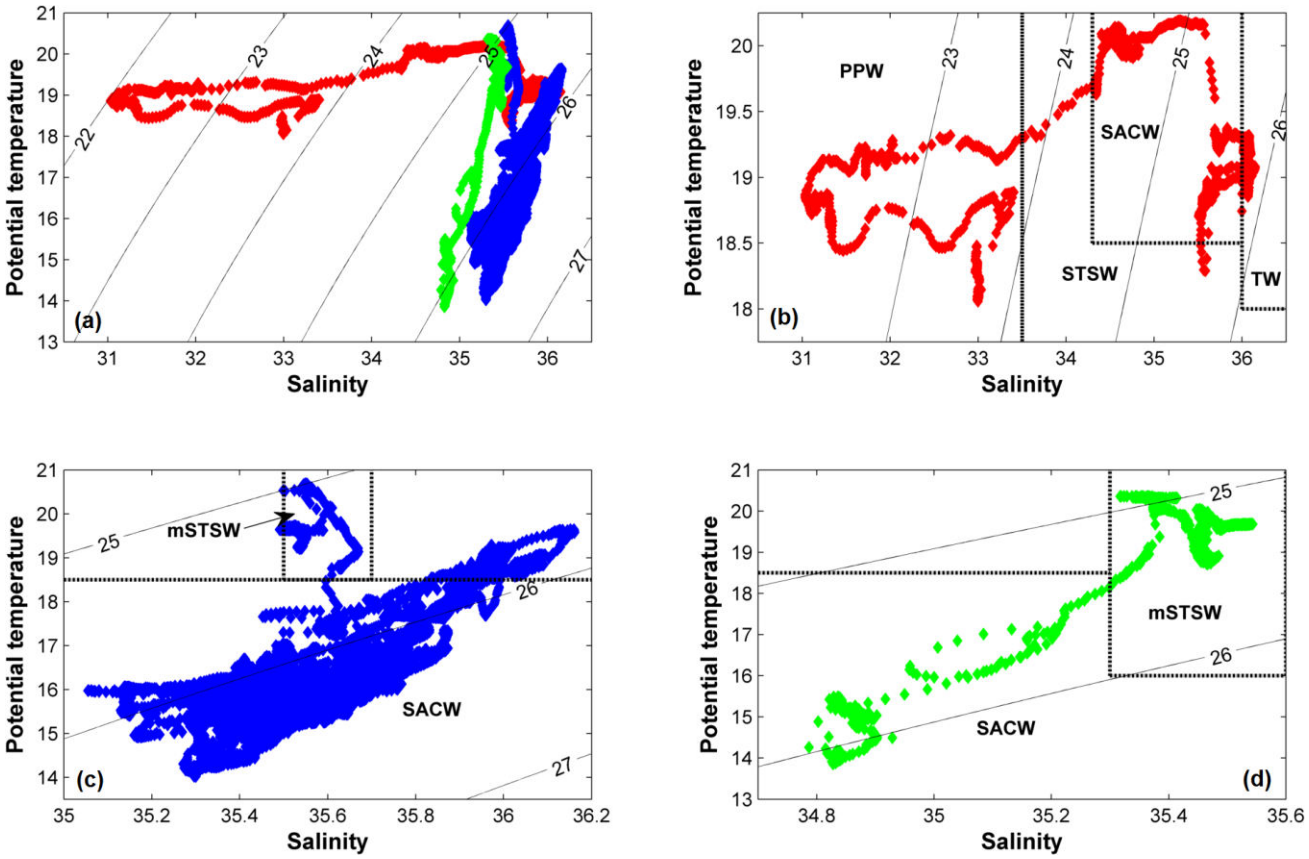

FIGURE 3 – Potential temperature vs salinity diagram of surface waters for (a) the whole study region, (b) South American shelf, (c) oceanic sub-region and (d) African shelf. The following water masses are identified: *Plata Plume Water* (PPW), *Subtropical Shelf Water* (STSW), *Tropical* Water (TW), *South Atlantic Central Water* (SACW), *modified Subtropical Surface Water* (mSTSW). The water mass indices follow Möller *et al.* (2008), Stramma & England (1999) and Gordon *et al.* (1987).

3.2 Longitudinal distribution of variables

Longitudinal distributions of fCO_2^{sw}, fCO_2^{atm}, SST, SSS, oxygen saturation and CSAT are shown in Figures 4 and 5 and mean values for each sub-region are presented in Table 3. The greatest variability of fCO_2^{sw} was found in coastal zones while the oceanic region was more homogeneous, but with mesoscale fluctuations (Figure 4a). Mean values (Table 3) for the whole region were 335.9 ± 9.6 µatm and 384.9 ± 4.8 µatm for fCO_2^{sw} and fCO_2^{atm}, respectively. Mean values of surface seawater and atmospheric fugacity were, respectively: 336.4 ± 16.9 µatm and 377.7 ± 0.8 µatm for the South American sub-region; 336.3 ± 8.1 µatm and 385.5 ± 4.6 µatm for the oceanic sub-region; 325.3 ± 16.7 µatm and 383.0 ± 0.9 µatm for the African sub-region.

SST showed variations along the cruise, with the highest value found in the African sub-region (Figure 4g), probably due to an eddy detached from Agulhas Current system. The oceanic region showed generally lower SST values than the adjacent coastal regions (Figure 4b). Mean SST (± standard deviation) for the entire cruise was 16.4 (± 1.4) ˚C, with sub-region averages as 19.2 (± 0.4) ˚C, 16.1 (± 1.0) ˚C and 18.8 (± 1.9) for the South American costal, oceanic and African coastal sub-regions, respectively. SSS (Figure 4c) was approximately uniform over the gyre (oceanic area) and dropped toward coastal regions, especially on the west. Mean (± standard deviation) SSS value for the entire cruise was 35.5 (± 0.5) and sub-regions means were 34.8 (± 1.6), 35.5 (± 0.2), and 35.3 (± 0.2) for the South American, oceanic and African sub-regions.

Surface oxygen saturation values ranged from about 90% to 100% for almost the entire cruise (Figure 4d) with a mean value (± standard deviation) of 95.4 (± 3.4) %. Relatively low saturation was found in specific areas such as near 15˚E (about 82.9 %), while the highest ones found in the African sub-region. CSAT variations along the cruise track are presented in in Figure 4e. The highest variations were found at about -42.5˚W and in the African shelf waters. Chlorophyll-a mean values obtained from seawater bottle samples are also depicted in Table 3.

TABLE 3: Mean ± standard deviation, minimum and maximum values for temperature, salinity, dissolved oxygen saturation, chlorophyll-a(*), CO_2 fugacity in surface seawater and atmosphere, ΔfCO_2, and sea-air CO_2 flux (W92 and T09) for the South American, oceanic and African sub-regions, and for the entire cruise. (*) Determined from surface seawater samples in CTD stations.

Region	SST [°C]	SSS	DO sat. [%]	Chl-a [mg m^{-3}]	fCO_2^{sw} [µatm]	fCO_2^{atm} [µatm]	ΔfCO_2 [µatm]	W92 [mmol CO_2 m^{-2} d^{-1}]	N00 [mmol CO_2 m^{-2} d^{-1}]	T09 [mmol CO_2 m^{-2} d^{-1}]
South American sub-region	19.2 ± 0.4	34.8 ± 1.6	92.0 ± 1.6	0.428 ± 0.2	336.4 ± 16.9	377.7 ± 0.8	-41.3 ± 17.5	-0.4 ± 0.2	-0.4 ± 0.2	-0.2 ± 0.1
	18.0	31.0	88.3	0.195	283.7	376.5	-95.2	-0.9	-0.9	-0.6
	20.2	36.1	96.4	0.810	359.9	380.0	-17.1	-0.1	-0.2	-0.1
Oceanic sub-region	16.1 ± 1.1	35.5 ± 0.2	95.5 ± 3.0	0.277 ± 0.2	336.3 ± 8.1	385.5 ± 4.6	-49.2 ± 8.1	-3.2 ± 2.2	-2.3 ± 1.4	-2.1 ± 1.4
	14.0	35.0	82.9	0.086	307.4	375.2	-75.4	-10.4	-7.0	-6.9
	20.7	36.2	103.5	0.693	363.6	393.2	-24.2	-0.1	-0.1	-0.1
African sub-region	18.8 ± 1.9	35.3 ± 0.2	99.5 ± 6.3	1.634 ± 2.2	325.3 ± 16.7	383.0 ± 0.9	-57.7 ± 17.0	-4.8 ± 1.5	-3.4 ± 1.1	-3.2 ± 1.0
	13.6	34.8	90.2	0.231	274.9	381.5	-109.5	-8.9	-6.4	-5.9
	20.3	35.5	119.3	4.881	379.6	384.9	-5.0	-0.4	-0.3	-0.3
Whole cruise values	16.4 ± 1.4	35.5 ± 0.5	95.4 ± 3.4	0.428 ± 0.6	335.9 ± 9.6	384.9 ± 4.8	-49.0 ± 9.7	-3.1 ± 2.2	-2.2 ± 1.5	-2.0 ± 1.5
	13.6	31.0	82.9	0.086	274.9	375.2	-109.5	-10.4	-7.0	-6.9
	20.7	36.2	119.3	4.881	379.6	393.2	-5.0	-0.1	-0.1	-0.1

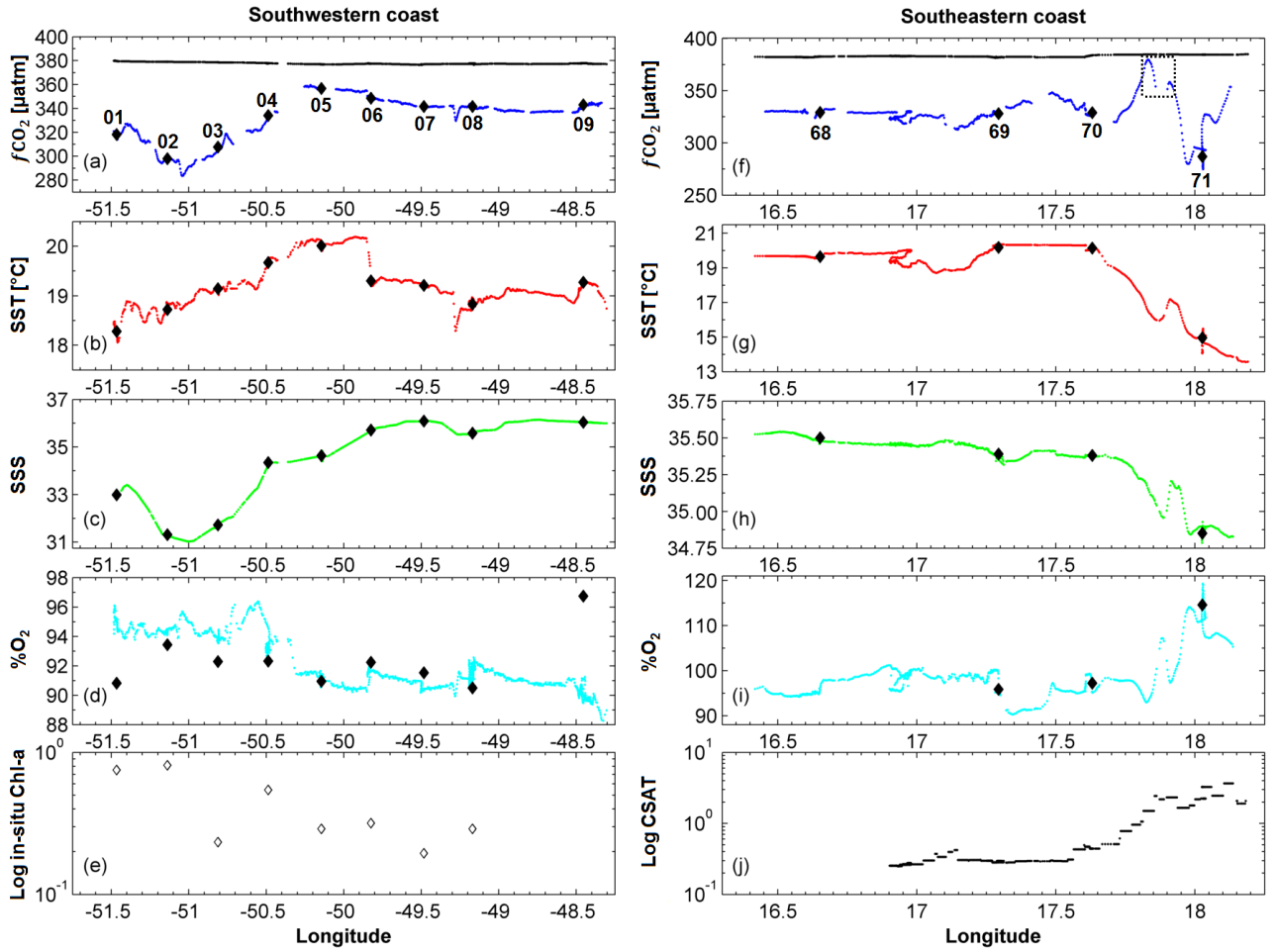

FIGURE 4 – Longitudinal distributions along South American sub-region (a-e, left column) and African sub-region (f-j, right column) of CO_2 fugacity in surface seawater (dark blue line) and atmosphere (black line), temperature (red line), salinity (green line), oxygen saturation (blue line), and log of chlorophyll (black diamonds are *in situ* chlorophyll data and black line is satellite retrieved). The dotted square highlights the region with the highest fCO_2^{sw} values in the entire cruise.

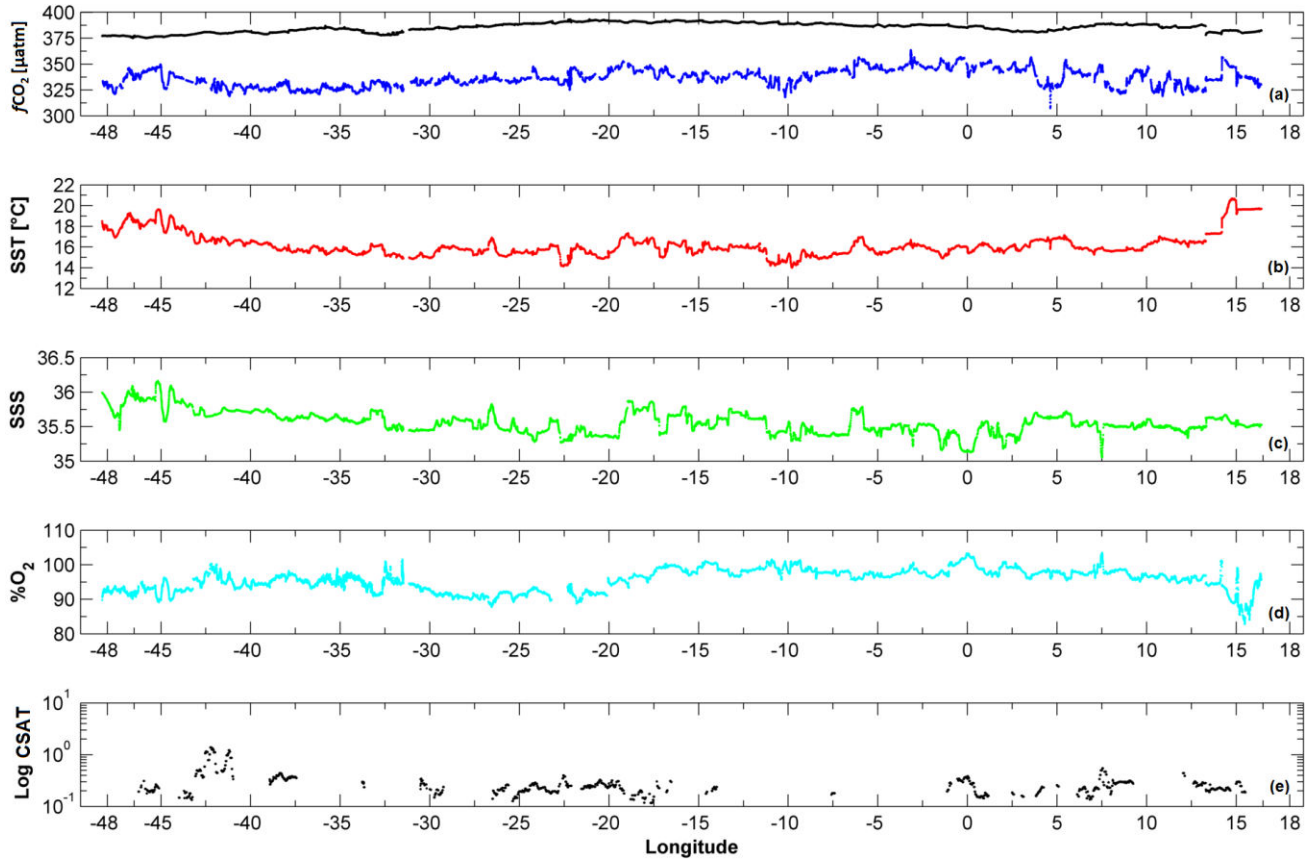

FIGURE 5 – Longitudinal distributions along oceanic sub-region of (a) CO_2 fugacity in surface seawater (dark blue line) and atmosphere (black line), (b) *in situ* temperature, (c) salinity, (d) oxygen saturation, and (e) log of chlorophyll-a (satellite retrieved).

3.3 Distribution of ΔfCO_2

The longitudinal ΔfCO_2 distribution was characterized by variations along the study area (Figure 6). The lowest ΔfCO_2 were measured in continental shelves waters (-95.2 µatm and -109.5 µatm for South American and African sub-region, respectively). Mean (± standard deviation) ΔfCO_2 value for the entire area was -49.0 ± 9.7 µatm. All ΔfCO_2 values were negatives, indicating that the sea surface was a sink for atmospheric CO_2 in the entire sampled region.

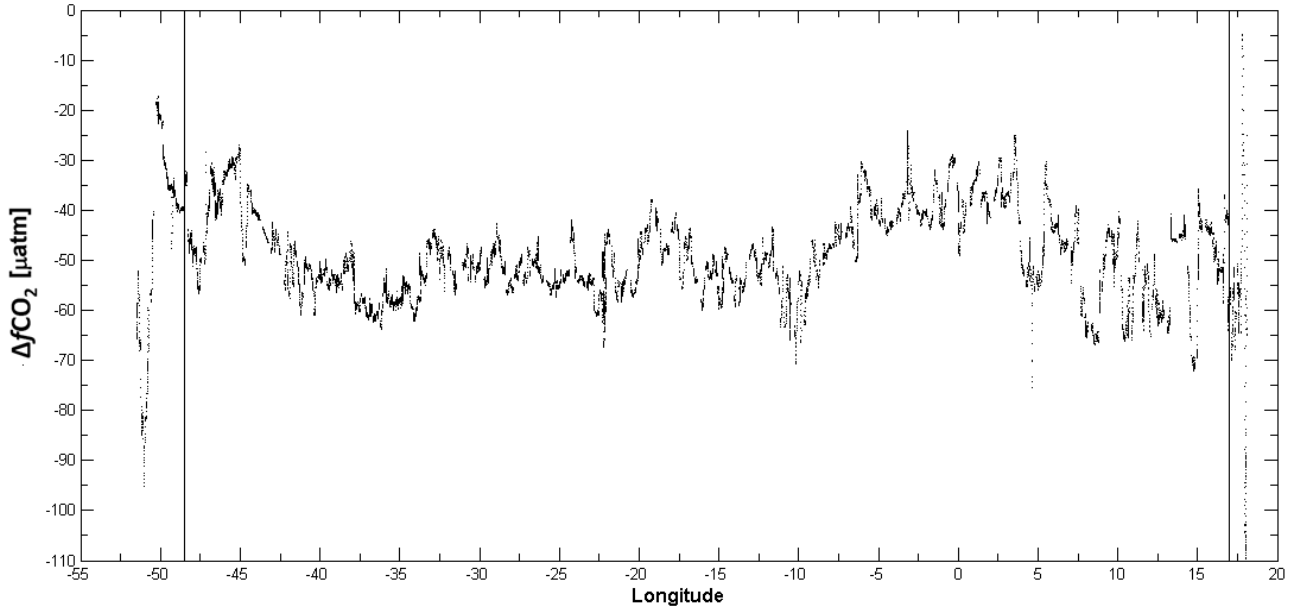

FIGURE 6: Longitudinal distribution of ΔfCO_2 along the entire cruise track. Vertical bars delimit the edge of continental slopes on the South American coast (left) and the African coast (right).

3.4 FCO_2 distribution

Figure 7 shows longitudinal variations in FCO_2 (using W92) along the cruise. The highest variations were found in the oceanic region (-10.4 to -0.1 mmol m^{-2} d^{-1}), followed by the eastern (right side of Greenwich, -8.8 to -0.4 mmol m^{-2} d^{-1}) and western (left side of Greenwich, -0.9 to -0.2 mmol m^{-2} d^{-1}) portions of the study area. Average sea-air CO_2 flux during the cruise was -3.06 ± 2.2 mmol m^{-2} d^{-1}, but with high spatial variability associated with mesoscale frontal structures (Figure 5 and 7), which are frequently observed along the Subtropical Convergence (Peterson & Stramma 1991; González-Silvera et al. 2004).

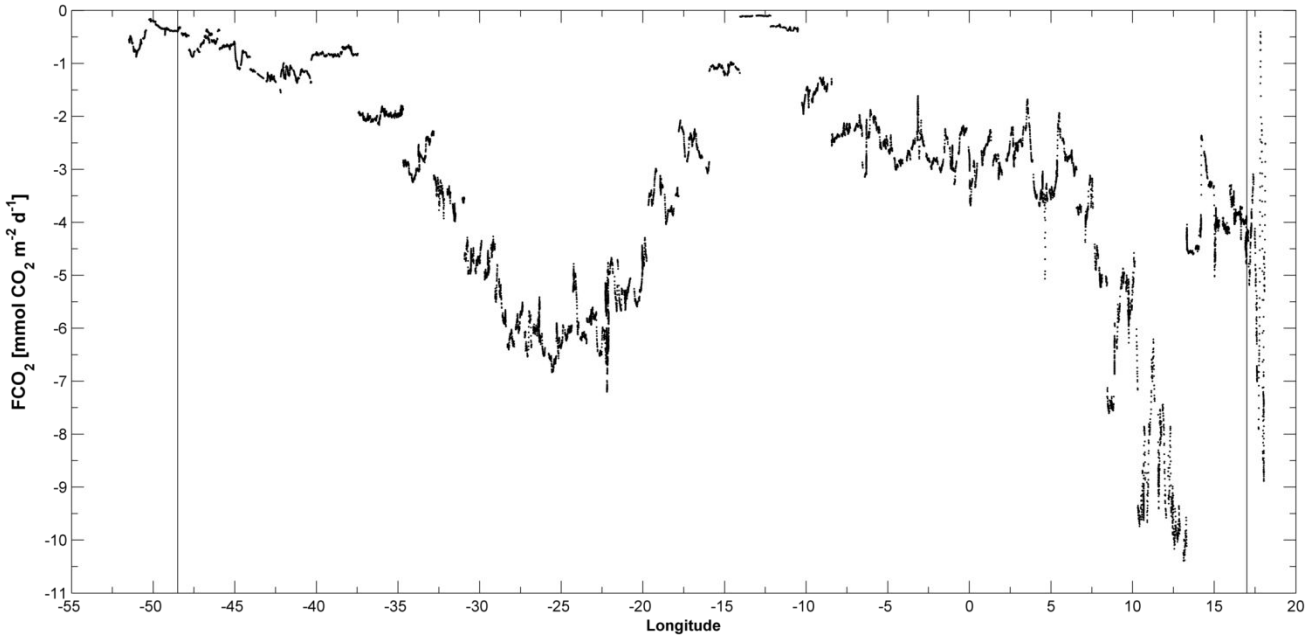

FIGURE 7 – FCO_2 (mmol CO_2 m^{-2} d^{-1}) longitudinal distribution using the transfer velocity coefficient by Wanninkhof (1992). Vertical bars delimit the end of the continental slope for the South American coast (left bar) and the African coast (right bar).

3.5 CO_2 fugacity and coupled biological-physical variables

Coupled physical-biological structures of the subtropical fronts most certainly influenced fCO_2^{sw} along the ship track. To calculate the temperature-normalized $\mathrm{fCO_2^{sw}}$ ($\mathrm{fCO^{sw}_{2\text{-}N16.4}}$) values, it was used the mean cruise temperature (16.4 ˚C), in order to evaluate the effect of temperature on $\mathrm{fCO_2^{sw}}$ distributions. Figure 8 shows results for each sub-region.

The greatest differences between $\mathrm{fCO_2^{sw}}$ and $\mathrm{fCO^{sw}_{2\text{-}N16.4}}$ (hereinafter f-fN) were in the South American sub-region (37.0 µatm), followed by the African (30.0 µatm) and the oceanic (4.0 µatm) sub-regions. The difference f-fN was equal to 0.09 µatm for the entire cruise.

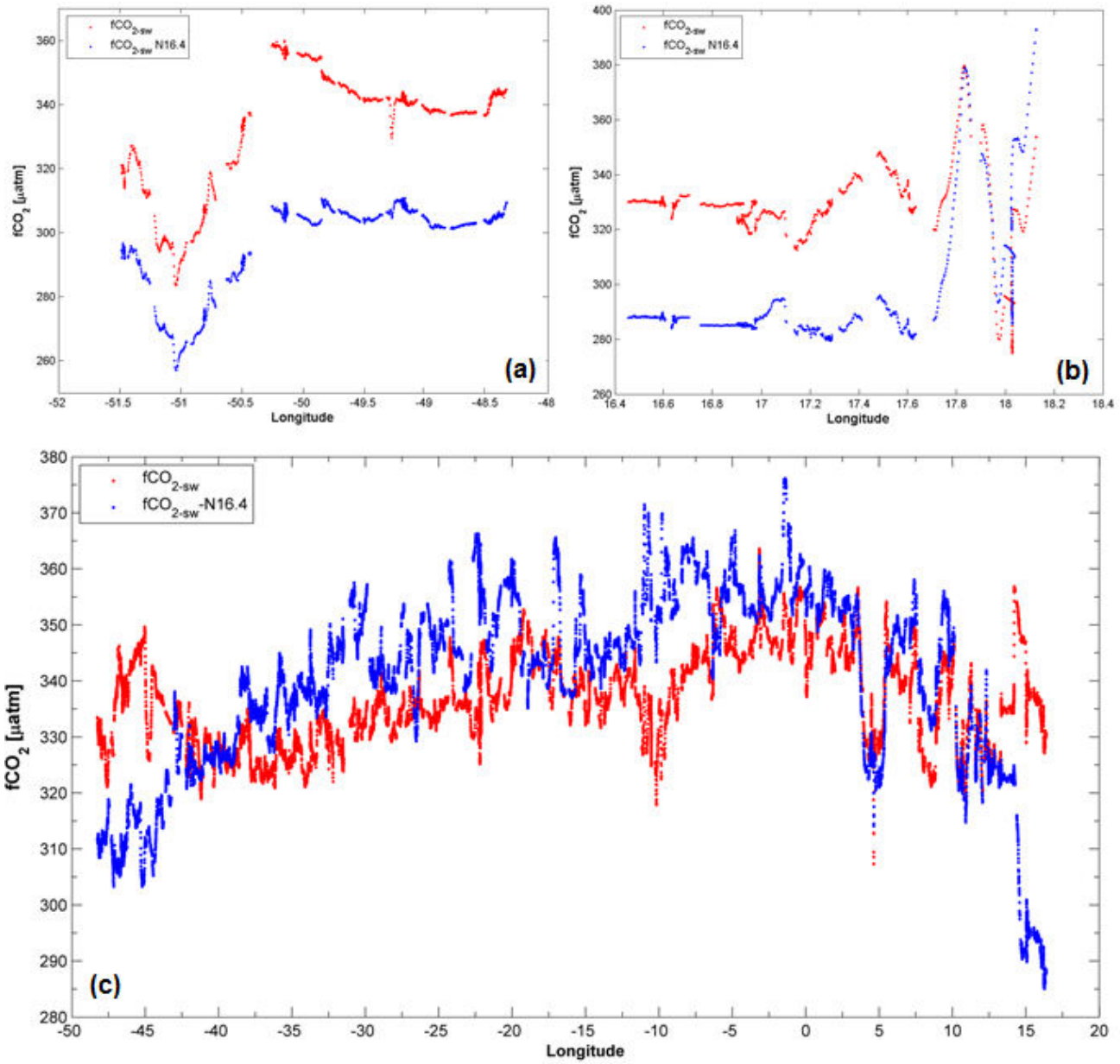

FIGURE 8 – CO_2 fugacity (fCO_2^{SW}, blue dots) vs normalized CO_2 fugacity to the mean cruise temperature of 16.4˚C ($fCO_{2-N16.4}^{SW}$, red dots) for the (a) South American, (b) African, and (c) oceanic sub-region.

Correlations between $fCO_{2\text{-}N16.4}^{SW}$ and temperature, salinity and chlorophyll-a were made for all available data (Figure 9) and for each sub-region (Figure 10). Considering the whole data set (Figure 9), $fCO_{2\text{-}N16.4}^{SW}$ was very well correlated (r = -0.893, N = 21428, p<0.001) with SST but weakly correlated with salinity and chlorophyll-a (r = 0.167 and -0.168, respectively). When each sub-region was considered separately (Figure 10), $fCO_{2\text{-}N16.4}^{SW}$ and salinity presented the highest correlation (r = 0.911, N = 1456, p<0.001) in the South American sub-region (Figure 10b). In the oceanic sub-region (Figures 11c-11e), $fCO_{2\text{-}N16.4}^{SW}$ correlated very well (r = -0.871, N = 15659, p<0.001) with temperature, followed by salinity (r = -0.676) and chlorophyll (r = -0.215). In the African region,

$fCO^{sw}_{2\text{-}N16.4}$ correlated reasonable well with chlorophyll and salinity (Figures 11g-11h), although, with opposite signs (r = 0.680, N = 586, p <0.001 and -0.629, N = 786, p< 0.001 respectively).

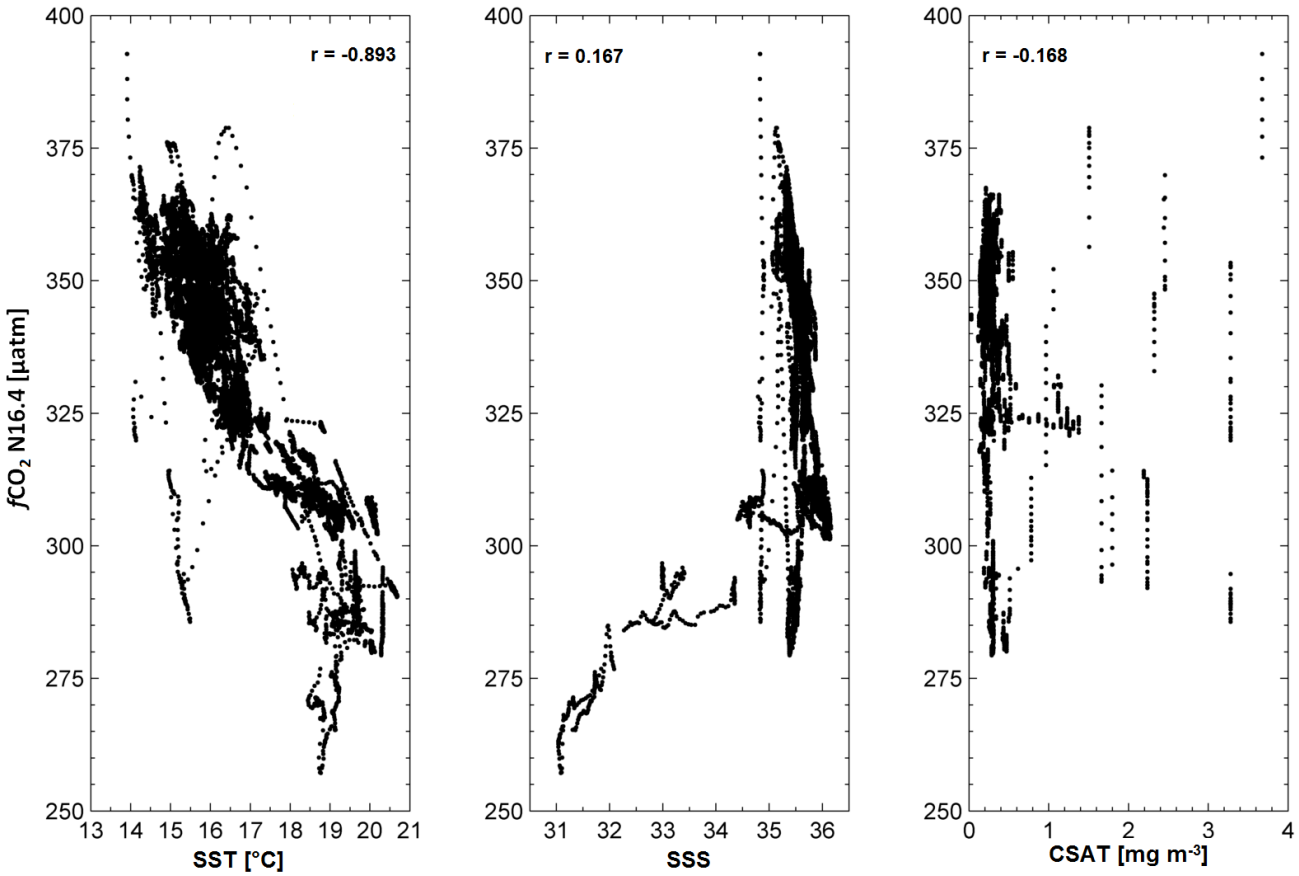

FIGURE 9 – Pearson's correlations between surface seawater CO_2 fugacity and (a) temperature, (b) salinity, and (c) chlorophyll (satellite) for all cruise data.

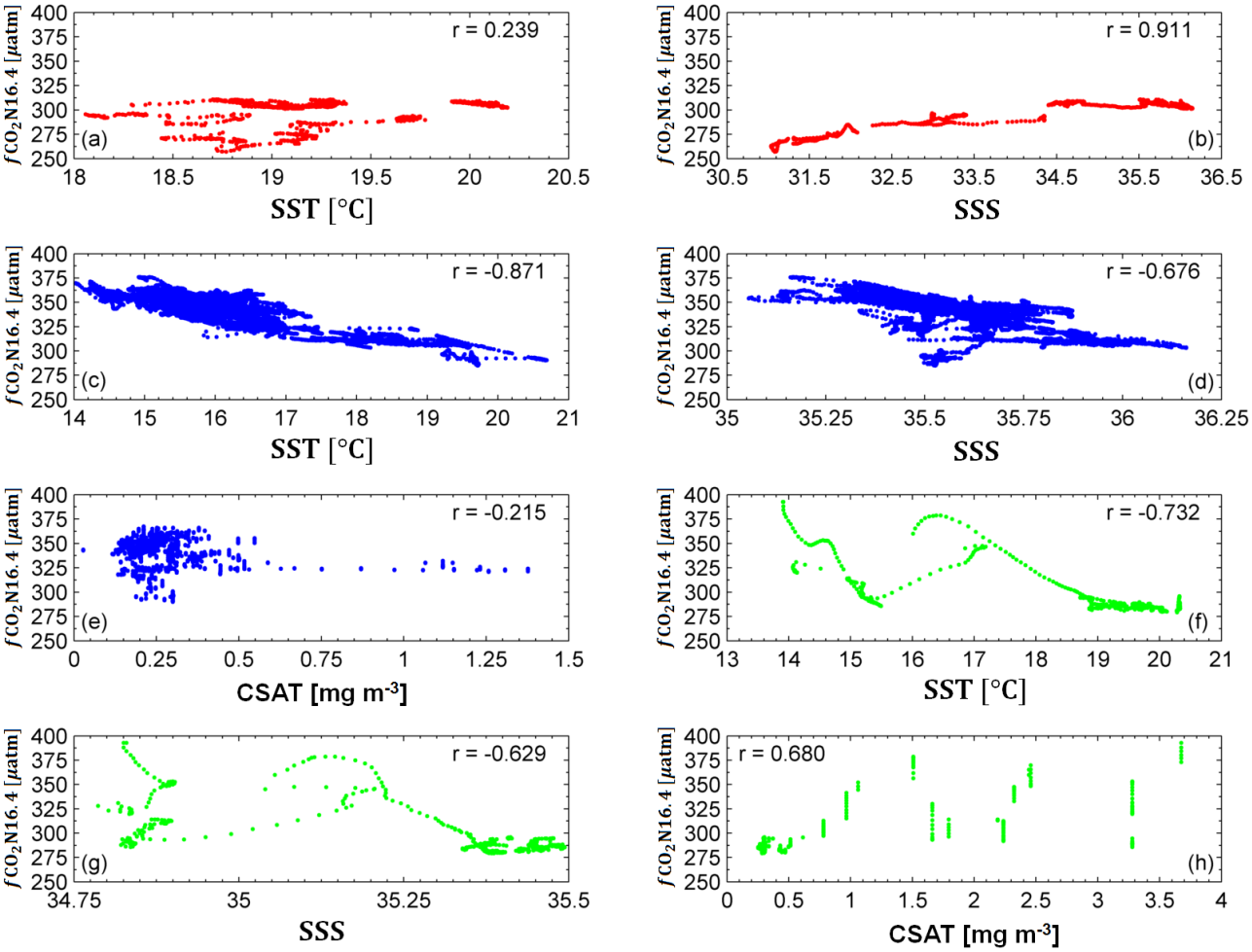

FIGURE 10 – Pearson's correlations between surface seawater CO_2 fugacity and temperature, salinity, and chlorophyll (satellite) for (a and b) the South American sub-region (red dots), (c to e) oceanic sub-region (blue dots), and (f to g) African sub-region (green dots). There was no available chlorophyll data from satellite for the South American sub-region due to cloudiness.

3.6 fCO_2^{sw} and $fCO_{2-N16.4}^{sw}$ Prediction models

Although correlations between fCO_2^{sw} and temperature were not linear (Figure 9), the MLR model could be used due to the quasi-Gaussian distribution of fCO_2^{sw}. An attempt to use GLM model was made using a Gaussian distribution (Triola *et al.* 2008; Zuur *et al.* 2009); However, no significant differences were found between coefficients determined by both MLR model and GLM models. Therefore, only results for the MLR model (Table 4 and Table 5) are presented.

The fCO_2^{sw} prediction model showed poor results (R^2 = 0.236), for the entire cruise data (Figure 11a). Therefore, no single linear relationship between sea surface temperature, salinity and chlorophyll could explain the observed fCO_2^{sw} values over the entire ship track. Among the sub-regions MRL models, the South American model (Figure 11b) showed the best result (R^2 = 0.885), followed by the oceanic model (R^2 = 0.322) and the African model (R^2 = 0.309). It must be noticed that for the South American model only SST and SSS data were used. As seen for the entire data

set, both the African and oceanic sub-regions fCO_2^{sw}values could not be significantly predicted by linear relationship between sea surface temperature, salinity and chlorophyll. The African sub-region model showed the highest standard error (Table 4), probably due to the strong dynamics of the region, influenced by an upwelling system and waters from the Agulha's Retroflection.

TABLE 4: Coefficients α, β1, β2, and β3 of fCO_2 prediction model, using a Multiple Linear Regression approach, for different regions. Determination coefficient, standard error and sample size are also shown for each region.(*) Only SST and SSS data were used in the South American sub-region.

Region	α	β1	β2	β3	R^2	Str. Err.	n
South American sub-region(*)	-261.9	-	16.0	8.4	0.885	5.976	1315
Oceanic sub-region	1152.1	-13.7	3.3	-24.4	0.322	6.122	6978
African sub-region	-2518.6	12.5	2.3	79.0	0.309	15.872	586
Cruise	660.5	-13.4	0.5	-9.2	0.236	8.250	7564

As $fCO_{2\text{-}N16.4}^{sw}$ models yielded better correlation coefficients than fCO_2^{sw} (data not shown), $fCO_{2\text{-}N16.4}^{sw}$ prediction models were developed for the same regions. These results (Table 5) were significantly better in comparison with the fCO_2^{sw} model. The entire cruise data model was highly improved (R^2 = 0.834), although the standard error value did not significantly decreased (8.196). The sub-regional models showed a similar pattern as for the previous models, with the South American sub-region presenting the best result (R^2 = 0.843), closely followed by the oceanic model (R^2 = 0.841), and then the African model (R^2 = 0.564). Respective standard errors were very similar to fCO_2^{sw}, with the highest values also found for the African model. Coefficients were, in general, higher in the $fCO_{2\text{-}N16.4}^{sw}$ model.

TABLE 5: Coefficients α, β1, β2, and β3 of $fCO_{2-N16.4}^{sw}$ prediction model, using a Multiple Linear Regression approach, for different regions. Determination coefficient, standard error and sample size are also shown for each sub-region.(*) Only SST and SSS data were used in the South American sub-region.

Region	α	β1	β2	β3	R^2	Str. Err.	n
South American sub-region(*)	5.5	-	1.6	7.5	0.843	5.261	1315
Oceanic sub-region	1461.6	-13.8	-10.3	-26.7	0.841	6.115	6978
African sub-region	-2475.6	13.11	-10.8	83.9	0.564	15.968	586
Cruise	1019.8	-14.7	-13.0	-13.1	0.834	8.196	7564

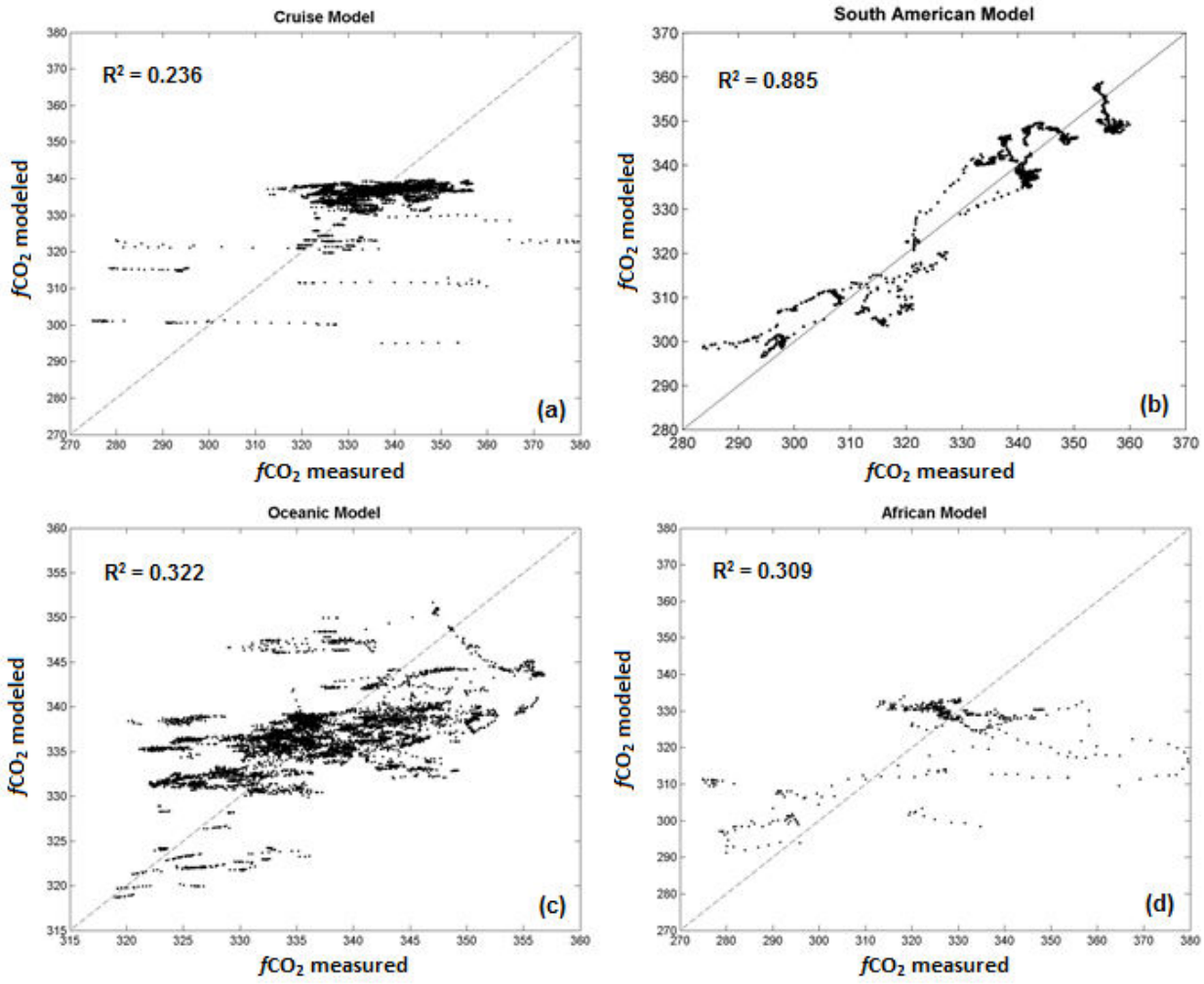

FIGURE 11 – Observed surface seawater CO_2 fugacity versus modeled surface seawater CO_2 fugacity for (a) all cruise data, (b) South American sub-region, (c) oceanic sub-region, and (d) African sub-region.

Other tests with the $\mathrm{fCO}_{2\text{-N16.4}}^{\mathrm{SW}}$ model were run by segmenting the sampling region westward, resulting in an increase of the determination coefficient. The best result (R^2 = 0.937, Std. Err. = 3.267, n = 4217) was found for the region constrained between 48.5°W and 20°W, which was also best among all presented results. This region comprises the oceanic area between South American shelf and the Mid Atlantic Ridge (Figure 2). The best-fit algorithm for this section was:

$$f\mathrm{CO}_{2-\mathrm{N16.4}}^{\mathrm{SW}}(20°\mathrm{W}) = 2421.4 - 8.941\ \mathrm{CSAT} - 3.628\ \mathrm{SST} - 56.8\ \mathrm{SSS} \qquad (8)$$

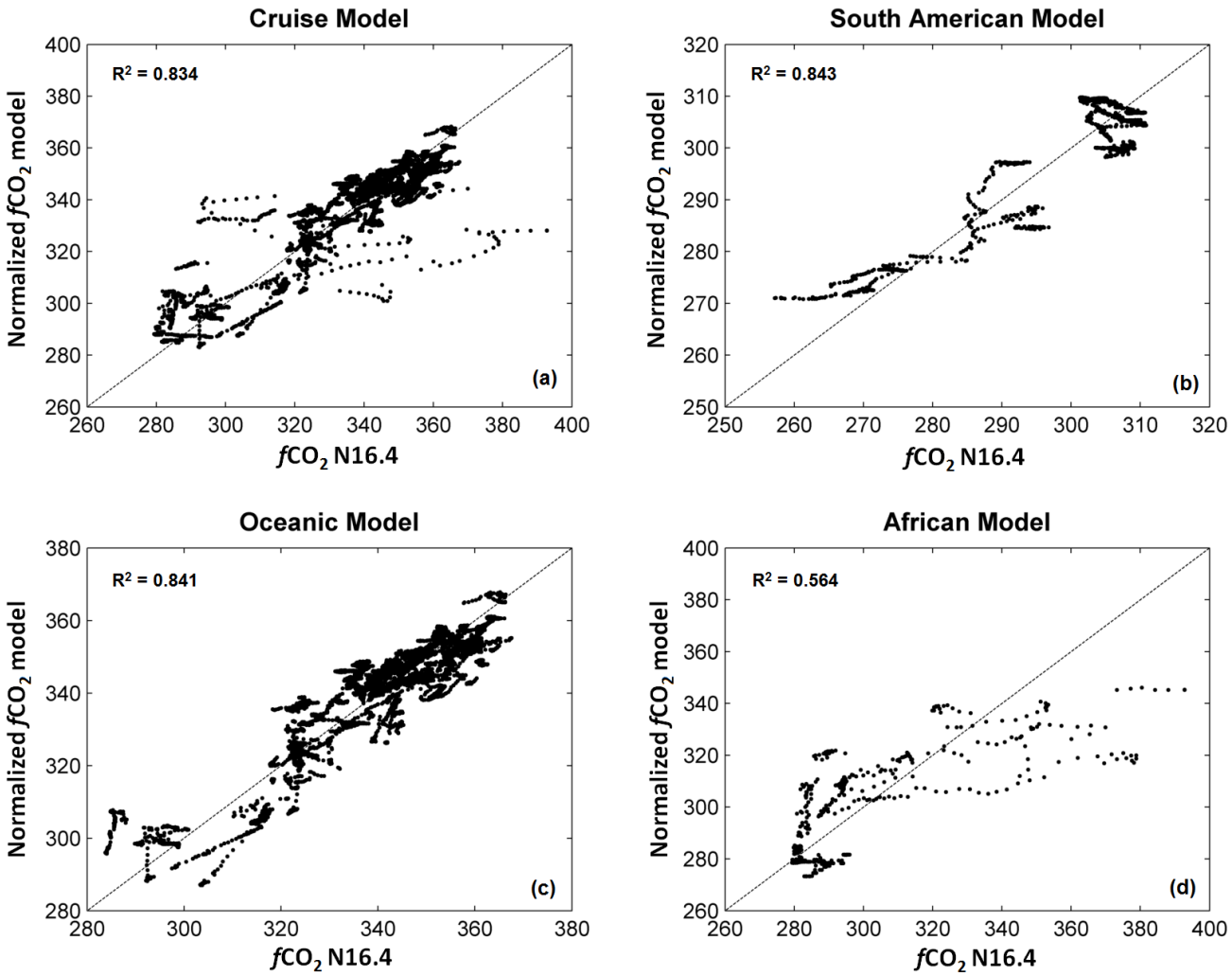

FIGURE 12 – $fCO_{2-N16.4}^{SW}$ versus modeled normalized CO_2 fugacity for (a) all cruise data, (b) South American sub-region, (c) oceanic sub-region, and (d) African sub-region.

4. Discussion

4.1 Characterization of the study area

Based on potential temperature-salinity diagrams (Figure 3), three sub-regions were identified in the study area: (1) South American sub-region, comprising the Southern Brazil continental shelf, slope and adjacent ocean (represented by one station at the beginning of the abyssal plane); (2) African sub-region, represented by the South Africa continental shelf, slope and adjacent ocean area; and (3) the oceanic sub-region, comprising the large area between the two sub-regions boundaries.

In the South American sub-region, PPW was found at surface in the first three CTD stations, which are located over the continental shelf zone (Figure 1). SACW was detected at the edge and middle of the continental slope and at the slope's base area (Figure 13). Based on temperature and

salinity values and distance from the continent, the presence of SACW at surface seems to be a result of the Brazil Current's meandering process (Stramma 1989, Peterson & Stramma 1991). TW was found in the oceanic section of this sub-region and at the slope, close to its base. The STSW, identified in the θ-S diagram is only apparent at the sea surface near the continental shelf break where encounters SACW (Figure 13) otherwise it is predominant below PPW over the shelf. SST data from stations (data not shown) demonstrate that STSW was under PPW cape in continental shelf region. The water masses distribution in this sub-region follows the pattern described in Möller *et al.* (2008).

In the oceanic sub-region (Figure 3c), SACW was the dominant water mass and mSTSW was identified in the easternmost portion of the region. However, high variations in thermohaline properties, especially temperature (Figure 5) were detected. Sea level anomaly (SLA) from altimetry data, from Chelton *et al.* (2011), were also analyzed for the same period of the cruise and the presence of eddies was detected. Figure 14 depicts two examples of eddy presence during the cruise period in the oceanic sub-region.

In the African sub-region, two main water masses were identified (Figure 3d and 13) and located at different areas. The mSTSW was seen from the adjacent ocean up to around 17.5°E, while SACW was found from after 17.5°E until over the continental shelf area. From Figure 13 (from e to g) it can be identified a typical sign of coastal upwelling water on the easternmost side where water with lower temperature and salinity are identified at sea surface (SACW) which is typically seen in this region and season (Liu *et al.* 2010 and references therein). The mSTSW is identified as the Subtropical Surface Water, originated in the Indian Ocean and modified after staying some time in Agulhas Retroflection zone where its thermohaline properties are slight changed and then transported to the South Atlantic Ocean by eddies or coastal jets at this region (Gordon *et al.* 1987).

4.2 Spatial distributions of fCO_2^{sw}, ΔfCO_2 and FCO_2

4.2.1 South America sub-region

In this sub-region, fCO_2^{sw} and ΔfCO_2 presented variation along the track (Figures 4a and 6), with two relatively low fCO_2^{sw} values in the mid shelf and slope (297.7 µatm in station 2, and 307.6 µatm in station 3). In the shelf zone, fCO_2^{sw} is very closely related to salinity as clearly demonstrate Figures 4a and 4c, whereas at the slope and in adjacent oceanic waters it is more related to surface temperature associated with oligotrophic waters of the Brazil Current, especially at the longitude of -49.7 where a strong variation can be identified in both Figures 4a and 4b.

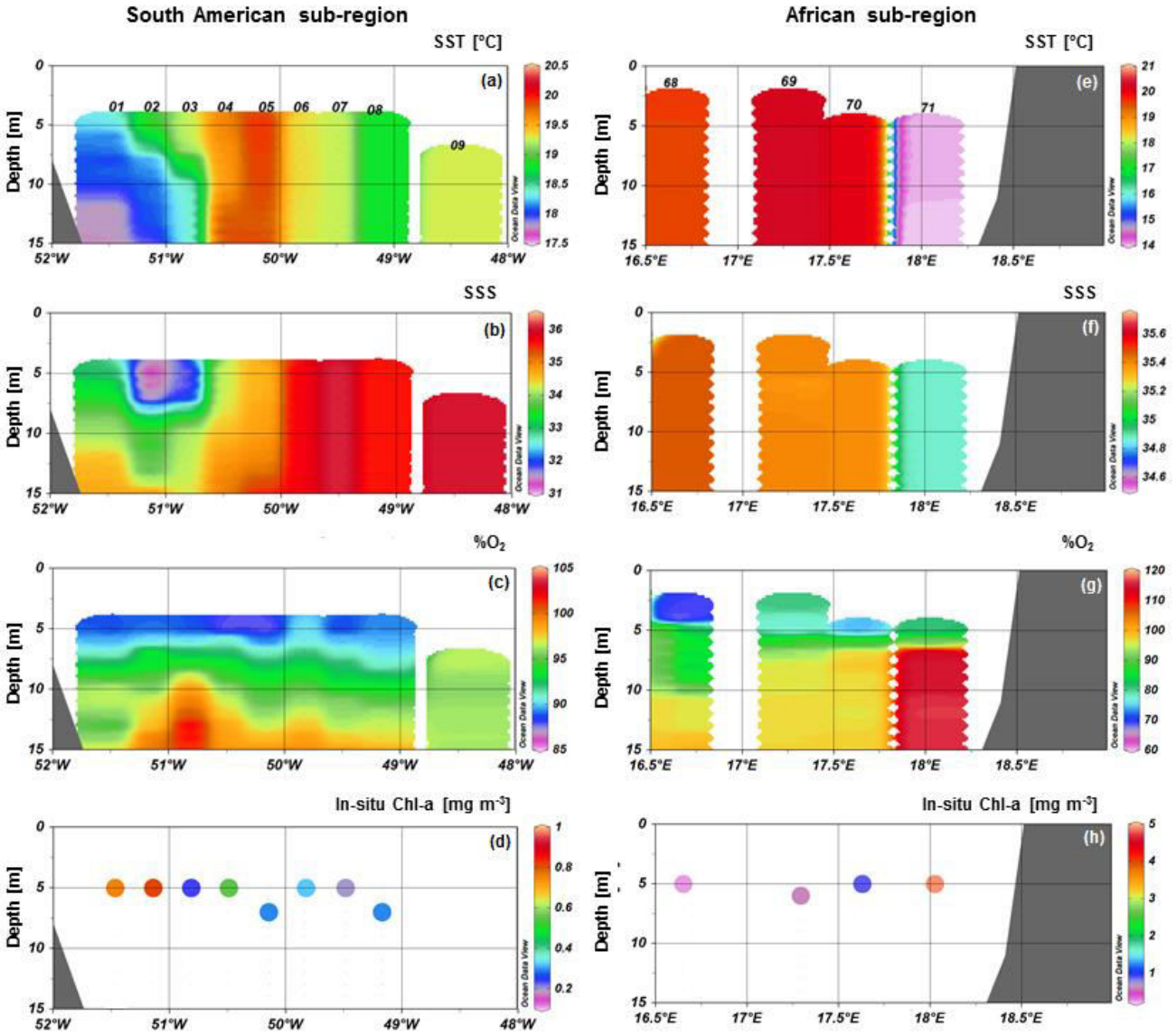

FIGURE 13 – CTD station profiles of sea surface temperature (a and e), salinity (b and f), oxygen saturation (c and g) and in-situ chorophyll-a (d and h) for the South American (left) and African (right) sub-regions.

The lowest fCO_2^{sw} coincides with the lowest salinity (31.31) and the highest chlorophyll concentration (0.810 mg m^{-3}) in this sub-region. SST and SSS values, in the shelf, are within those characteristic of PPW waters, which transports high concentrations of nutrients derived from La Plata River outflow, enhancing biological productivity on the shelf through lateral mixture (Muelbert *et al.* 2008). Historical hydrographic data reveal that PPW can undergo large amplitude spatial displacements, reaching far north, beyond 26°S during winter season (Möller *et al.* 2008). This seasonal fluctuation influences primary production in the area, with high chlorophyll-a concentration along the coastal zone in southern Brazilian waters (Garcia & Garcia 2008). Hence, biological activity over the continental shelf certainly influenced the observed fCO_2^{sw} values over the shelf where PPW waters was observed.

The highest fCO_2^{sw} in the sub-region was measured at station 5 in the slope, and corresponds to both lowest ΔfCO_2 magnitude (-20.3 µatm) and highest SST (20.01 °C). Chlorophyll-a concentration and oxygen saturation (0.289 mg m^{-3} and 90.9%, respectively) were lower than values surrounding station 5 (0.544 mg m^{-3}, 92.3% for station 4 and 0.318 mg m^{-3}, 92.2% for station 6, respectively). This lower phytoplankton biological activity indicates that a less effective drawdown of fCO_2^{sw} in comparison with the vicinity. In this location, SACW waters were found which are transporting fewer nutrients to the region than PPW. At the mid slope area a conspicuous decrease in fCO_2^{sw} was registered (Stations 7 to 8, Figure 4a) probably in response to surface temperature trend (Figures 5a and b). This close relation with temperature is in agreement to the temperatures effect on fCO_2^{sw} (Goyet *et al.* 1993). This minimum is associated with a local minimum of chlorophyll concentration.

All measurements of ΔfCO_2 were negative, indicating that the sea acts as a sink of atmospheric CO_2. Highest FCO_2 (W92) values were found over the continental shelf (-0.75 and -0.65 mmol m^{-2} d^{-1} at stations 2 and 3, respectively). Mean FCO_2 for this sub-region was -0.4 mmol m^{-2} d^{-1}, characterizing the South American sub-region as a sink area, driven by biological and physical (salinity) factors over the continental shelf as result of the PPW water influence, and by temperature in the slope and adjacent ocean where warmer and less productive waters are found.

Ito, R.G. (personal communication, 2014) conducted a CO_2 study that includes a ship track very close to the one presented in this sub-region, but in late spring, under higher temperatures and lower salinities. The fCO_2^{sw} distribution was very similar, although values were all higher than in the present work. This suggests the dominance of temperature effect over fCO_2^{sw}. Jiang *et al.* (2008) conducted a similar study in the U.S. South Atlantic Bight (SAB), located at the same latitudes in the northern hemisphere. In the same seasonal period, ΔfCO_2 range (minimum of -45 µatm, and maximum of 55 µatm) in SAB was greater than in our study (minimum -81 µatm, and maximum of -61 µatm). Monthly net CO_2 fluxes calculated (N00) in April in SAB ranged between -4.1 mmol CO_2 m^{-2} day^{-1} (mid shelf) and -4.4 mmol CO_2 m^{-2} day^{-1} (outer shelf) while in this work the average for mid and outer shelf was -0.4 mmol CO_2 m^{-2} day^{-1}. Discrepancies are probably related to differences in the regional dynamics and flora composition of the respective coastal waters. The SAB is a region dominated by large salt marsh zones, which releases large amounts of carbon and nutrients, whereas in the South American sub-region, apparently the biological factor is less importance probably due to the fact that PPW waters are retreating at that time of the year, being its nutrient and carbon content lost likely almost consumed.

4.2.2 Oceanic sub-region

The fCO_2^{sw} in the oceanic sub-region presented a high variability along the track (Figures 5a). The mean fCO_2^{sw} was 336.3 ± 8.0 µatm, increasing towards the Greenwich line from both directions. The lowest values (<325 µatm) were found in the western section of this sub-region which coincided with slightly lower temperature (~15.9 °C) and higher chlorophyll-a concentration (~0.292 mg m^{-3}), in comparison with the eastern side (~16.7 °C and ~0.243 mg m^{-3}). In the southeastern Atlantic Ocean, anti-cyclonic eddies generated at the Agulhas Retroflection are frequent and they can be trapped between Walvis Ridge and South Africa coast for some time before continuing their track northwestwards (e.g. Lutjeharms & Van Ballegooyen 1988; Doglioli *et al.* 2007). On the other hand, the southwestern side is affected by eddies (either cyclonic or anti-cyclonic) from Brazil-Malvinas Confluence (e.g. Lentini *et al.* 2006; Saraceno & Provost 2012), as well as mesoscale features from the Subtropical Front (Peterson & Stramma 1991). Both cyclonic eddies and frontal features are responsible for nutrients transport and/or upwelling and enhance primary productivity (McGillicuddy & Robinson 1997; Gonzalaz-silvera *et al.* 2008). Hence, the relatively low temperature and high chlorophyll are favorable conditions for a greater atmospheric CO_2 uptake through solubility (temperature effect) and biological pump (photosynthesis) (Goyet *et al.* 1993; Libes 2009) on the western side. Overall, the average ΔfCO_2 (-49.8 µatm, Figure 6) found for the southwestern side of the oceanic sub-region was slightly higher than the southeastern sector (-47.3 µatm).

Between ~42.5°W and ~30°W (Figure 5a), there was an area of lower fCO_2^{sw} values (~327.7 µatm), associated with a lower temperatures, and, more noticeable, with a higher oxygen saturation (~95%), and relatively high chlorophyll-a concentration (~0.448 mg m^{-3}) (Figures 5d and 5e). The $f - fN$ distribution (Figure 8c) indicates that biological factors were controlling fCO_2^{sw} at the west end of this area, whereas, in the middle and easternmost end temperature had a greater effect. One significant drop in fCO_2^{sw} was seen around 10°W (~329.3 µatm), corresponding to stations 38-40 (Figure 2), associated with a SST decrease (1.3°C between stations 38 and 40, Figure 5b). In addition, an increase in both oxygen saturation and chlorophyll concentration (97.8% and 0.204 mg m^{-3} at station 38, 101.1% and 0.454 mg m^{-3} at station 40) were also found in this sector. SLA data (Figure 14) showed an anti-cyclonic and a cyclonic eddies on the way between stations 38 and 40, respectively. In this section, both physical and biological factors seem to have driven the fCO_2^{sw} decrease (Figure 8c).

At the eastern end, a significant fCO_2^{sw} drop was observed between ~3°E and 5°E (Figure 5a), corresponding to stations 53 to 55, associated with an increase in temperature between both stations (Figure 5b). Salinity also presented a slight increase in this area (Figure 5c). Chlorophyll concentrations dropped between those two stations (0.365 mg m^{-3} and 0.155 mg m^{-3}, respectively),

while oxygen saturation increased in comparison with vicinities, though with values slightly undersaturated (98.3% and 97.8%, respectively). Based on Figure 8c, biological factors appeared to have more influence on fCO_2^{sw} as $fCO_{2-N16.4}$ did not change patter and $f - fN$ was only 2.5 µatm. Probably there was a high biological activity event prior to the cruise in that section, responsible for the observed drop in fCO_2^{sw}.

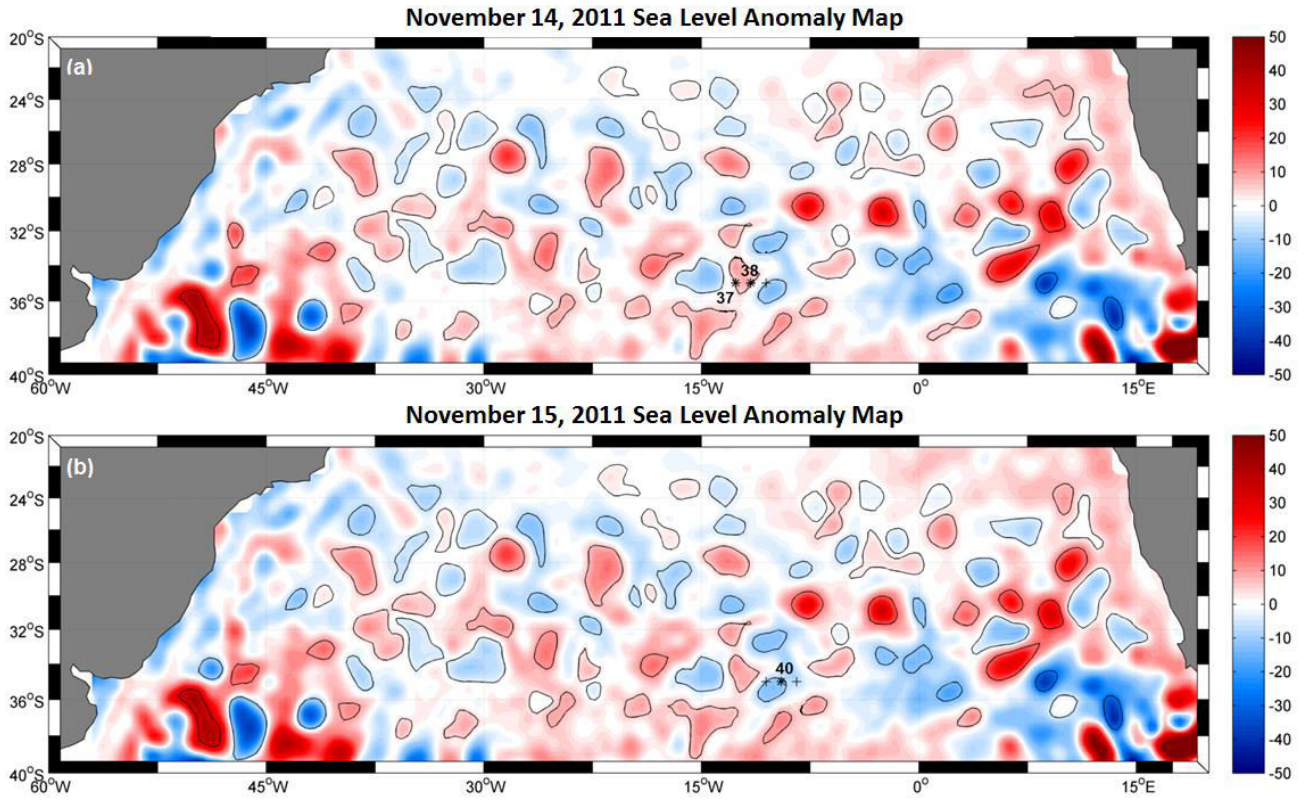

FIGURE 14 – Sea level anomaly (SLA) images for (a) November 14, and (b) 15 of 2011, representing eddy features crossed during the cruise period. Altimetry data used from Chelton *et al.* (2011). The sign * means station inside the eddy, and + on the outside the eddy.

Other study in the North Atlantic Subtropical (NAS) gyre by Andersson *et al.* (2013) found similar magnitudes as observed in this work. ΔfCO_2 values reported for June (a warm month in the Northern Hemisphere) ranged from -35 µatm to -45 µatm (35°N), while data in our study show a greater amplitude, from -24 µatm to -75 µatm. This could indicate that the South Atlantic Ocean absorbs more atmospheric CO_2 during warm months. In that study, the 35°N latitude was a watershed line between low latitudes and high latitudes waters. This division meant a difference on mean ΔfCO_2 for these two areas with ΔfCO_2 < -30 µatm (-30 µatm to -45 µatm) at low latitudes, and ΔfCO_2 > -30 µatm (~0 µatm to -30 µatm) at high latitudes. In the present studied we attempt to see a similar division longitudinally, however, no significant difference in the amplitude of ΔfCO_2 was found when comparing west (-70.8 µatm to -24.2 µatm) and east (-75.4 µatm to -25.1 µatm) portions of the oceanic sub-region, which suggest that at 35°S the ocean behaves fairly equal.

The ΔfCO_2 in this work showed a greater amplitude (-24.2 µatm to -75.4 µatm), than data presented by Takahashi *et al.* (2009) (-25.4 µatm to -44.8 µatm, in November) at 36°S latitude in the Atlantic Ocean, which was the closest to the study area. The entire oceanic region at this latitude presented negative ΔfCO_2 for the same period (or month) as in the present study. However, our values indicate that the ocean may be absorbing an order of magnitude less atmospheric CO_2, -0.02 mol C m^{-2} $month^{-1}$ (-2.1 mmol CO_2 m^{-2} d^{-1}, Table 3), than -0.2 mol C m^{-2} $month^{-1}$ calculated by Takahashi *et al.* (2009). It is worth mentioning, however, that the Takahashi *et al.*'s data for this region is relatively poor and most probably a result of interpolation from a larger dataset. Therefore, our results may represent updated and more realistic data.

As stated above, the entire oceanic sub-region showed negative ΔfCO_2 (average = -49.2 ± 8.1 µatm), indicating that this region was considerably undersaturated, favoring atmospheric CO_2 absorption. The region is an important CO_2 sinking area with a mean FCO_2 (W92) of -3.1 ± 2.2 mmol m^{-2} day^{-1}.

4.2.2.1 CO_2 fugacity and eddies: An observation

During the cruise in the oceanic sub-region, the ship crossed nine eddies (7 cyclonic and 2 anti-cyclonic) that were identified by altimetry data (Chelton *et al.* 2011). For simplicity, in this work, only three eddies have been analyzed: two cyclonic (stations 20, and 40), and one anti-cyclonic (stations 37 and 38).

In cyclonic eddies, $f - fN$ were 13.8 µatm (station 20) and 27.3 µatm (station 40), suggesting temperature's influence, however, with different importance over fCO_2^{sw} distribution. At station 20, Figure 8c shows that SST is the dominant factor controlling fCO_2^{sw}, since no change in fCO_2^{sw} pattern was observed. fCO_2^{sw} values increase 4 µatm in comparison to surroundings, indicating subsurface water uplifting that were undersaturated (93%). Oxygen saturation profile shows that this water has the same properties over the first 10m. Yet a substantial CO_2 drawdown (ΔfCO_2 = -50.6) occurred, as a moderate chlorophyll-a concentration (0.343 mg m^{-3}) was found in this station. It appears that eddy-pumping was in its early stages, as oxygen saturation was still very low, covering biological production (Arístegui *et al.* 1997; McGillicuddy & Robinson 1997; Chen *et al.* 2008). On the opposite in station 40, temperature had some influence over fCO_2^{sw}, given $f - fN$ high value of 23.7 µatm, but it was not the dominant factor. Thus the high chlorophyll-a (0.448 mg m^{-3}) and oxygen saturation (101%) are result from cyclonic eddy nutrient pumping associated, enhancing primary productivity which yielded a significant drawdown of atmospheric CO_2 (ΔfCO_2 = -56.7 µatm) (Arístegui *et al.* 1997; McGillicuddy & Robinson 1997).

Stations 37 and 38 were sampled within an anti-cyclonic eddy. Temperature was the main property driving fCO_2^{sw} pattern in both stations, even with low $f - fN$ values (4.6 µatm and 8.8 µatm respectively). As expected chlorophyll concentration and oxygen saturation were lower than

vicinities. A low biological activity is expected, due to deepening of the thermocline at the cyclonic ring, nevertheless there was atmospheric CO_2 uptake as ΔfCO_2 values (-50.4 µatm and -46.8 µatm) demonstrate. This suggests that effect of mesoscale features over biogeochemical properties may be more complex and in need of more clarification as some studies already indicate (Mahadevan *et al.* 2002, Chen *et al.* 2008, Guidi *et al.* 2012).

4.2.3 African sub-region

In the African sub-region, fCO_2^{sw} (Figure 4f) declined from oceanic (329.0 µatm at station 68) to continental (286.8 µatm at station 71) waters. fCO_2^{sw} values were in agreement with ranges in previous works in the same region and season (González-Dávila *et al.* 2009; Santana-Casiano *et al.* 2009, Monteiro et al 2010). The ΔfCO_2 also decreased towards the continent, ranging from -53.2 µatm (station 68) to -97.6 µatm (station 71). Both chlorophyll concentration and oxygen saturation values (Figures 5i-j and 13f) showed opposite trends, both increasing towards the continental shelf, with the highest values at station 71 (4.881 mg m^{-3} and 115.5% respectively) due to a high biological productivity (Hutchintons *et al.* 2009). The abrupt changes in all observed parameters (Figures 5f-j and 14, right column) over the continental slope is due to the offshore frontal zone of the Benguela system, located around the 500 m isobath (Monteiro *et al.* 2010).

The highest fCO_2^{sw} (379.6 µatm) was found in an area enclosed by stations 70 and 71, over the African continental slope. In this zone fCO_2^{sw}, temperature, salinity, and oxygen saturation fluctuated (Figure 4f-i), and two peaks of fCO_2^{sw} were found (Figure 4f, dashed square). Figure 8c shows that those peaks had little influence from temperature. Both SST and SSS reach their local maxima (Figures 4g and 4h) while fCO_2^{sw} decreased. Filaments are recurrent features in the offshore domains of upwelling systems, being also responsible for upwelling of deeper waters and impacting CO_2 uptake either by absorption of atmospheric CO_2, or by carbon export (Lutjeharms *et al.* 1991; Arístegui *et al.* 2007). Moreover, warm-core eddies and filaments, originated in the Agulhas Retroflection, can reach this location in the South Atlantic Ocean with important impacts on the African coastal zone (Dumcombe Rae *et al.* 1992; Hutching *et al.* 2009). Therefore, the region between stations 70 and 71 must have alternated between cold (high Chlorophyll-a and oxygen saturation values) and warm filaments (low Chlorophyll-a and oxygen saturation). The first by cold upwelling and rich DIC waters through vertical mixing, enhancing fCO_2^{sw}, and the second by transporting warmer and saltier waters with lower DIC content.

The lowest fCO_2^{sw} value (274.9 µatm) was found at station 71 (SST 14.9 °C and in-situ chlorophyll 4.881 mg m^{-3}, Figure 13 e and h) associated with mean oxygen saturation of 114.6%. Average ΔfCO_2^{sw} was -97.6 µatm (ranging from -67.2 µatm to -109.5 µatm), configuring this region as a potentially high sink of atmospheric CO_2. The $f - fN$ was expressive (18.1 µatm), confirming

the expected effect of temperature on fCO_2^{sw}, but, as Figure 8b shows, this was not the prevailing factor as the pattern did not change around that station. Given the high chlorophyll-a and oxygen saturation values at station 71, it is reasonable to state that the main mechanism driving CO_2 uptake was primary productivity, followed by the physical factor. Our results are in agreement with Gregon & Monteiro (2013) which pointed out that the main factors controlling surface fCO_2^{sw} in the southern Benguela upwelling system were primary production, CO_2 exchange (physical factor), and calcification. The calculated FCO_2 (W92) for the African sub-region was -4.8 ± 1.5 mmol m^{-2} d^{-1}, characterizing this region as a strong atmospheric CO_2 sink for that period, driven primarily by biological factors and secondarily by physical factors.

Santana-Casiano *et al.* (2009) measured similar fCO_2^{sw} values, ranging from ~240 µatm to ~310 µatm in the same month and around the same latitude as in the present study. Similarly, a reduction in temperature and salinity was observed in the vicinities of Cape Peninsula Cell (34°S) and Cape Columbine (33°S) due to upwelled water from intermediate depths. It was pointed out that the mean annual FCO_2 (-0.71 mol m^{-2} yr^{-1}) indicates southern Benguela system is a moderate sinking zone during warm seasons. González-Dávila *et al.* (2009) also reported negative fluxes for this region (-3.24 mol m^{-2} yr^{-1}) when CO_2 drawdown was mainly result of biological responses. Our results corroborate to the high productive nature of upwelling systems such as the southern Benguela system (Hutchintons *et al.* 2009; Monteiro et al 2010). However, recent studies have suggested this system is a weak sink of atmospheric CO_2, due to a balance between reducing fCO_2^{sw} processes at surface (primary productivity and CO_2 exchange) and enhancing fCO_2^{sw} processes at bottom (mainly remineralization) (Gregon & Monteiro 2013).

4.3 Physical and biological contributions

Based on results from the correlations between fCO_2^{sw} and temperature, salinity and chlorophyll, and the $f - fN$ analysis of values and patterns, an attempt was made to assess the physical and biological contributions to observed fCO_2^{sw} for each sub-region.

Mean $f - fN$ in the South American sub-region (37.0 µatm) was the highest among the three sub-regions, implying that SST had the greatest influence on fCO_2^{sw} here. The $fCO_{2-N16.4}^{sw}$ pattern shown in Figure 8a indicates that temperature was not the dominant factor on fCO_2^{sw}, except for an area around -49.25°W. This region is located at the continental slope just southeast of Rio Grande Cone region, where irregularities at bottom topography induce water column instability. Therefore temperature would be driving fCO_2^{sw} in this particular area due to mixing resulted by mesoscale instabilities (Nardi, 2013). However salinity (and chlorophyll-a) was better correlated to $fCO_{2-N16.4}^{sw}$ than temperature (Figures 11a and 11b). This was probably an indirect effect of low salinity PPW on phytoplankton activity, since this water carries high nutrient levels, promoting phytoplankton production (Muelbert *et al.* 2008). This effect is demonstrated in Figures 4a and 4c as fCO_2^{sw} closely

follows SSS. Influence of river discharge has also been evident at other locations, either decreasing fCO_2^{sw} such as the Amazon river (Ternon *et al.* 2000), or increasing fCO_2^{sw}, as in the South Atlantic Bight (Jiang *et al.* 2008), and Gulf of Maine (Signorini *et al.* 2013). Those results demonstrate that the CO_2 uptake in the South American sub-region is highly controlled by physical factors (salinity and temperature, respectively), followed by a biological factor (primary productivity).

In the oceanic sub-region, $f - fN$ values were a little higher than 4.0 µatm in the entire area, indicating a weak influence of SST on fCO_2^{sw}, although a few areas showed greater SST influence, such as between -48.°W and 42, and ~10°W – ~6°W (Figure 8c). In general the western portion had a slightly higher SST influence ($f - fN$ = 6.4 µatm), than the eastern side (4.2 µatm). SST and SSS correlations with $fCO_{2-N16.4}^{sw}$ indicate that physical factors were the main drivers of CO_2 uptake (Figure 10c to 10e). Colder and fresher waters are from higher latitudes, bearing higher chlorophyll concentrations, and are driven to this region either by the STF, or by cyclonic eddies, enhancing atmospheric CO_2 absorption (Peterson & Stramma 1991; Gonzalez-Silvera *et al.* 2004; Chelton *et al.* 2011). Based mainly on the correlations results, it was possible to state that the CO_2 uptake during this cruise area was mainly dominated by physical factors (temperature and salinity) followed by biological factors.

In the African sub-region $f - fN$ was around 30.9 µatm (Figure 8c) but in the Benguela upwelling zone it reached 7.7 µatm, which indicates a lower influence of SST over fCO_2^{sw}. Correlation coefficients calculated between fCO_2^{sw} and SST, SSS and chlorophyll pointed to temperature as the main parameter governing fCO_2^{sw} spatial distribution, but closely followed by chlorophyll and salinity. Using only data from CTD stations (not shown), station 71 was shown to act as an outlier. If this is dropped from the analysis, SSS is highly correlated (R = 0.996) to fCO_2^{sw}, followed by temperature (-0.795), and chlorophyll's (0.283). Based on these results, it is suggested that physical factors are the main drivers of fCO_2^{sw} distribution in oceanic waters, whereas in the shelf area biological factors control fCO_2^{sw}. In fact, the shelf region is governed by the biological pump followed by CO_2 exchange (solubility pump), in agreement with recent findings in Gregon & Monteiro (2013).

4.4 Prediction model of fCO_2^{sw} and $fCO_{2-N16.4}^{sw}$

Considering the entire cruise data, MRL yielded relatively poor results mainly due to the heterogeneity of the study area, which encloses three very dynamically and biogeochemically distinct regions: a coastal region with riverine influence on the western side of the cruise track (Gonzales-Silvera *et al.* 2004; Möller *et al.* 2008; Garcia & Garcia 2008; Liu *et al.* 2010), an upwelling coast on the eastern side (Santana-Casiano *et al.* 2009), and an oceanic region with high incidence of mesoscale features (Peterson & Stramma 1991; Chelton *et al.* 2011). Horizontal outlying dots (Figure 11a) represent mainly areas at the shelves and mid slope of the African sub-region, including its frontal zone around mid-slope (Santana-Casiano *et al.* 2009; Monteiro 2010).

Those regions show high spatial and temporal variability, so larger data coverage would probably improve this model. Moreover, other works have used additional variables to generate $\mathrm{pCO_2}$ /$f\mathrm{CO_2}$ models, such as geographical coordinates (Lefèvre *et al.* 2003), or total dissolved inorganic carbon (DIC) and alkalinity (ALK) (Signorini *et al.* 2013). Adding more parameters would probably enhance a model that represents of a single track as $f\mathrm{CO}_2^{sw}$ is affected by diverse properties. The use of $f\mathrm{CO}_{2-\mathrm{N16.4}}^{\mathrm{sw}}$ in the model showed a significant improvement (Table 5) even for the whole data set.

The best $f\mathrm{CO}_2^{sw}$ model result was for the South American sub-region (Figure 11b), since both variables were highly (SSS, r = 0.837) or fairly (SST, r = 0.578) correlated with $f\mathrm{CO}_2^{sw}$. Although it is a highly dynamic environment as observed before, fluctuations in the variables along the shelf did not affect the model. The $f\mathrm{CO}_{2-\mathrm{N16.4}}^{\mathrm{sw}}$ model (Figure 12b) is weaker than $f\mathrm{CO}_2^{sw}$ model, probably due to removal of the temperature effect, but, as salinity is the main factor controlling $f\mathrm{CO}_2^{sw}$, the model was still fairly good.

Result for oceanic sub-region model reflects the heterogeneity of this area. Outliers in Figure 11c are mainly representative of the eastern sector of the sub-region which is known for mesoscale features, such as eddies, that can greatly alter $f\mathrm{CO}_2^{sw}$ values particularly at the border due to vertical mixing (Hood *et al.* 2001; Mahadevan *et al.* 2002). Unfortunately no eddy structure was identified from SLA images in the vicinities of these stations, although at the eastern side SLA anomalies were more intense than at the western side. The $f\mathrm{CO}_{2-\mathrm{N16.4}}^{\mathrm{sw}}$ model showed an improvement (Figure 12c, Table 5) over the $f\mathrm{CO}_2^{sw}$ model.

The African sub-region model presented the highest standard error (Table 5) which can be clearly seen in Figure 11d. This sub-region encompasses two very different areas, the Benguela upwelling system (Santana-Casiano *et al.* 2009) and an oceanic region with high occurrence of eddies, mainly anti-cyclonic ones (Gordon *et al.* 1987; Clement & Gordon 1995). This heterogeneity of water masses, with cold upwelling waters and warmer waters in the oceanic region, partially explains the poor model results. In this sub-region, mainly physical factors drive $f\mathrm{CO}_2^{sw}$ in the oceanic area, whereas shelf area is driven primarily by biological factors.

The $f\mathrm{CO}_{2-\mathrm{N16.4}}^{\mathrm{sw}}(20°\mathrm{W})$ model showed the best result among all presented models. The outliers observed in the $f\mathrm{CO}_2^{sw}$ model are considerably reduced. The region encompassed represents the western portion of the Mid Atlantic Ridge. SLA images showed that the eastern sector had more intense positive and negative anomalies than the western one in the cruise period, translating in less variability. Both regions differ in terms of dynamic, where the west shows lower incidence of anti-cyclonic eddies (warms and poor waters, but it is influenced by the STF which generates colder, fresher and richer waters (Gordon et al 1987, Peterson & Stramma 1991; Gonzalez-Silvera *et al.* 2004). The removal of eastern side of study area,explains the improvement in the model performance.

It is clearly observable that the removal of the temperature effect ($fCO_{2-N16.4}^{sw}$) enables a better correlation between fCO_2^{sw} and other variables. As temperature is used to calculate fCO_2^{sw}, when removed, its correlation is no longer predominant, allowing other parameters, such as chlorophyll-a, to stand out more. The oceanic sub-region, presenting the most stable temperature values, had the higher improvement when calculated $fCO_{2-N16.4}^{sw}$ model. An attempt to create a model considering data normalization for the whole cruise was made (equation 9) and a quadratic relation between it and temperature:

$$fCO_2^{sw-mod} = \alpha_0 + \alpha_1 CSAT + \alpha_2 SSS + SST[\alpha_3 + \alpha_4 SST + CSAT.(\alpha_5 + \alpha_6 SST) + SSS.(\alpha_7 + \alpha_8 SST)]$$

In which, the coefficients are respectively: 554.0 (α_0), -8.0 (α_1), -7.1 (α_2), 6.9 (α_3), 0.7 (α_4), -0.2 (α_5); -0.01 (α_6), -0.2 (α_1), and -0.01 (α_1).

The model showed poor results (Figure 15), superestimating them. This is could be related to not consideration of other factors, such as biological. More tests, data consideration and discussions must be made as, to our knowledge, there is no article wrote about it. Nonetheless, this perspective fCO_2^{sw} modeling could favor fCO_2^{sw} prediction and comparison between environments.

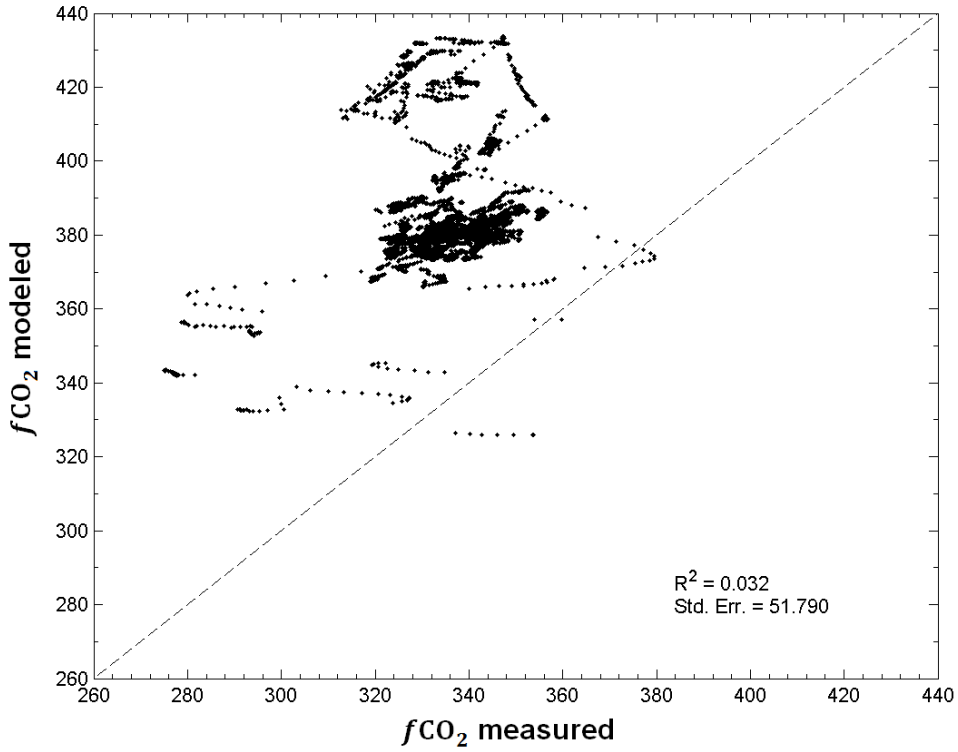

FIGURE 15 – Observed surface seawater CO_2 fugacity versus modeled surface seawater CO_2 fugacity considering normalization of fCO_2^{sw} data for the whole cruise area.

5. Summary and conclusion

An analysis of fCO_2^{sw}, ΔfCO_2, and consequent FCO_2 over the latitude of 35°S in South Atlantic Ocean and adjacent shelves was made. This are region not very frequently sampled, especially the South America and oceanic. During the cruise period, all regions behaved as CO_2 sinks, with the African and South America sub-regions presenting the strongest ΔfCO_2 values, respectively. The presence of dynamic processes demonstrate clear influence over biological and physical parameter which, in turn, governed fCO_2^{sw} distribution. PPW was the main factor controlling it in South America sub-region, while Benguela upwelling system was the one in the African sub-region. In oceanic sub-region meandering from STF and eddies were the dynamic factors controlling SST and SSS which were the main parameters controlling CO_2 absorption. The present work corroborate with the idea of temperate South Atlantic as an important CO_2 sink, as well as the African sub-region demonstrated in previous studies. South American shelf showed to be a strong sink fits into the external shelf group, which are considerable CO_2 absorbers.

The fCO_2^{sw} models showed poor results as they do not represented well the highly physically and biogeochemically dynamic regions encompassed. A fCO_2^{sw} model for the west side of the Mid Atlantic Ridge showed the best fit between all models generated. South America sub-region also presented very good results, only considering SST and SSS. A new look over fCO_2^{sw} modeling showed better results when using normalized fCO_2^{sw} data. Unfortunately, the first attempt to generate a fCO_2^{sw} model considering this kind of data was not successful. To our knowledge, this is the first time a group worked over this point of view. Further tests and considerations of how incorporate other parameters should be made to try improving the model. The present work bring new CO_2 data for the South Atlantic region, especially in the southwestern zone.

4. SÍNTESE DOS RESULTADOS

4.1. DISTRIBUIÇÃO DA fCO_2^{sw}, ΔfCO_2^{sw} E FCO_2

Alta variabilidade nos valores de fCO_2^{sw} e, consequentemente, ΔfCO_2 e FCO_2 foi observada ao longo de toda a região de estudo, sendo que as médias (± desvio padrão) encontradas para todo cruzeiro foram iguais a 335.9 (± 9.6) µatm, -49.0 (± 9.7) µatm e -3.1 (± 2.2) mmol m^{-2} dia^{-1} (W92), respectivamente. As maiores flutuações foram encontradas nas regiões costeiras, sendo que as maiores diferenças para fCO_2^{sw} (mínimo de 274.9 µatm e máximo de 379.6 µatm) e ΔfCO_2^{sw} (-109.5 µatm e -5.0 µatm) foram encontradas na costa africana. Diferenças atribuídas ao contraste entre o sistema de ressurgência da Corrente de Benguela e ao oceano adjacente. Os fluxos médios (± desvio padrão, W92) encontrados em cada sub-região foram -0.4 (± 0.2) mmol m^{-2} d^{-1} para costa sul-americana, -3.2 (± 2.2) mmol m^{-2} d^{-1} para a região oceânica e -4.8 (± 1.5) mmol m^{-2} d^{-1} para a costa africana. Logo, todas as regiões atuaram como sumidouros de CO_2 atmosférico durante o período do cruzeiro. Este resultado corrobora com outros que sugerem o oceano Atlântico Sul temperado (Takahashi *et al.* 2002, 2009) e plataformas continentais de latitudes intermediárias como sumidouros de CO_2 (Cai *et al.* 2006; Chen & Borges 2009; Laruelle *et al.* 2010).

4.2. CONTRIBUIÇÕES DOS PROCESSOS FÍSICOS E BIOLÓGICOS

Baseado nos resultados da análise das diferenças entre fCO_2^{sw} e $fCO_{2-N16.4}^{sw}$, padrões de distribuição das propriedades analisadas e correlações, determinou-se os processos que mais influenciam a distribuição do fCO_2^{sw} e, consequentemente, o FCO_2 para toda a região de estudo e para cada sub-região analisada. Na região da plataforma sul-americana, fCO_2^{sw} demonstrou alta relação com a salinidade (r = 0.911), suportada pela análise de $f - fN$ que sugeriu forte influência da SST, porém não dominante sobre fCO_2^{sw}. Atividade biológica também apresentou forte influência, devido à presença de águas da PPW. Para a sub-região oceânica, parâmetros físicos (r = -0.871 para SST e r = -0.676 para SSS) foram os principais fatores controladores da fCO_2^{sw} na região, seguido da concentração de clorofila-a. Na sub-região africana, a análise de $f - fN$ mostrou a influência da variável biológica (r = 0.680) como maior contribuinte na variação do fCO_2^{sw} na região de plataforma, enquanto que, no oceano adjacente, a temperatura teve maior influência, seguido pela salinidade. A presença de vórtices durante o período do cruzeiro e sua influência sobre fCO_2^{sw} pode ser observada na região oceânica, promovendo absorção de CO_2 atmosférico devido a processos de mistura vertical e horizontal relacionados à dinâmica específica de vórtices.

4.3. MODELO DA FUGACIDADE DE CO_2

Os resultados do modelo MLR para previsão de fCO_2^{sw} mostraram-se insatisfatórios para toda região de estudo (r^2 = 0.236, erro padrão (EP) = 8.250). Resultado provavelmente por abranger três regiões muito distintas dinâmica e biogeoquimicamente (Longhurst 1995). Os valores mais contrastantes do modelo geral correspondem à região da plataforma africana. As sub-regiões também mostraram resultados insatisfatórios, exceto para a sub-região sul-americana (R^2 = 0.885, EP = 5.976), provavelmente devido à alta correlação de fCO_2^{sw} com as variáveis físicas. Os modelos de previsão de $fCO_{2-N16.4}^{sw}$ mostraram melhores resultados em todas as regiões, exceto para região sul-americana (R^2 = 0.843, EP = 5.261). Os resultados mais satisfatórios foram para a região oceânica (R^2 = 0.841, EP = 6.115) e todo o cruzeiro (R^2 = 0.834, EP = 8.196). Um modelo considerando a região entre 48.5°W 2 20°W mostrou o melhor resultado (R^2 = 0.937, EP = 3.267). Tal região corresponde à zona oceânica a oeste da cordilheira meso-Atlântica. Um modelo considerando a normalização dos dados de fCO_2^{sw} foi gerado, entretanto, os resultados superestimam os valores.

5. CONCLUSÕES

No presente estudo, a análise da distribuição do fluxo líquido de CO_2 na interface oceano-atmosfera ao longo da latitude de 35°S do oceano Atlântico Sul e plataformas continentais adjacentes demonstrou que, para o período analisado, o oceano comportou-se como um sumidouro de CO_2 atmosférico. Esta afirmação baseia-se nos relativamente altos valores de fCO_2^{sw} e ΔfCO_2^{sw} (todos negativos) calculados ao longo de toda a região de estudo. Avaliação preliminar sobre as variáveis e consequentemente mecanismos, que estavam influenciando a distribuição de fCO_2^{sw} foi realizada, com a conclusão de que temperatura e salinidade foram os principais condutores da variabilidade da fugacidade do CO_2, enquanto que a atividade biológica (clorofila-a) apresentou pequenas contribuições à exceção da região africana. A elaboração de um único modelo preditivo de fCO_2 para toda a região de estudo mostrou-se inviável. Contudo bons resultados foram encontrados para o modelo preditivo de $fCO_{2-N16.4}^{sw}$ para praticamente todas as regiões analisadas. O melhor modelo (R^2 = 0.937, EP = 3.267, n = 4217) encontrado obteve-se ao se restringir a região a ser modelada, em especial, na porção sudoeste da área de estudo.

REFERÊNCIAS

Andersson, J.A.; L.A. Krug; N.R. Bates; S.C. Doney. 2013. Sea–air CO2 flux in the North Atlantic subtropical gyre: Role and influence of Sub-Tropical Mode Water formation. *Deep-Sea Research II*, 91:57–70.

Aminghafari, M.; N. Cheze; J.-M. Poggi. 2006. Multivariate denoising using wavelets and principal componente analysis. *Computational Statistics and Data Analysis*, 50:2382–2398.

Arístegui, J.; P. Tett; A. Hernández-Guerra; G. Basterretxea; M.F. Montero; K. Wild; P. Sangrá; S. Hernández-León; M. Cantón; J.A. García-Braun; M. Pacheco, and E.D. Barton. 1997. The influence of island-generated eddies on chlorophyll distribution: a study of mesoscale variation around Gran Canaria. *Deep-Sea Research I*, 44:71–96.

Arístegui, J.; E.D. Barton; D.A. Hansell. 2007. Contribution of upwelling filaments to offshore carbon export in the subtropical Northeast Atlantic Ocean. *Limnology Oceanography*, 52(3):1287–1292.

Bianchi, A.A.; L. Bianucci; A.R. Piola; D.R. Pino; I. Schloss; A. Poisson, and C.F. Balestrini. 2005. Vertical stratification and air-sea CO_2 fluxes in the Patagonian shelf. *Journal of Geophysical Research*, 110:C07003, doi:10.1029/2004JC002488.

Bianchi, A.A.; D.R. Pino; H.G.I. Perlender; A.P. Osiroff; V. Segura; V. Lutz; M.L. Clara; C.F. Balestrini and A. R. Piola. 2009. Annual balance and seasonal variability of sea-air CO_2 fluxes in the Patagonia Sea: Their relationship with fronts and chlorophyll distribution.

Borges, A.V.; B. Delille; M. Frankignoulle. 2005. Budgeting sinks and sources of CO_2 in the coastal ocean: diversity of ecosystems counts. *Geophysical Research Letters*, 32, L14601. doi: 10.1029/2005GL023053.

Bozec, Y.; H. Thomas; K. Elkalay; H.J.W. de Baar. 2005. The continental shelf pump for CO_2 in the North Sea – evidence from summer observation. *Marine Chemistry,* 93:131–147.

Braga, E.S.; V.C. Chiozzini; G.B.B. Berbel; J.C.C. Maluf; V.M.C. Aguiar; M. Charo; D. Molina; S.I. Romero; B.B. Eichler. 2008. Nutrient distributions over the Southwestern South Atlantic continental shelf from Mar del Plata (Argentina) to Itajaí (Brazil): Winter– summer aspects. *Continental Shelf Research*, 28:1649–1661.

Cai, W.-J.; M. Dai, and Y. Wang. 2006. Air-sea exchange of carbon dioxide in ocean margins: A province-based synthesis. *Geophysical Research Letters*, 33, L12603, doi:10.1029/2006GL026219.

Chelton, D.B.; M.G. Schlax; R.M. Samelson. 2011. Global observations of non-linear mesoscale eddies. *Progress in Oceanography*. 91(2):167–216.

Chen, C.-T.A. & A.V. Borges. 2009. Reconciling opposing views on carbon cycling in the coastal ocean: Continental shelves as sinks and near-shore ecosystems as sources of atmosphericCO2. *Deep-Sea Research II*, 56:578–590.

Chen, F.; W.-J. Cai; Y. Wang; Y.M. Rii; R.R. Bidigare; C.R. Benitez-Nelson. 2008. The carbon dioxide system and net community production within a cyclonic eddy in the lee of Hawaii. *Deep-Sea Research I*, 55:1412–1425.

Chen, L.; S. Xu; Z. Gao; H. Chen; Y. Zhang; J. Zhan, and W. Li. 2011. Estimation of monthly air-sea CO_2 flux in the southern Atlantic and Indian Ocean using in-situ and remotely sensed data. *Remote Sensing of Environment*, 115:1935–1941.

Chierici, M.; A. Fransson; D.R. Turner; E.A. Pakhomov, and P.W. Froneman . 2004. Variability in pH, fCO_2, oxygen and flux of CO_2 in the surface water along a transect in the Atlantic sector of the Southern Ocean. *Deep-Sea Research II*, 51:2773–2787.

Chierici, M.; A. Olsen; T. Johannessen, J. Trinañes; R. Wanninkhof. 2009. Algorithms to estimate the carbon dioxide uptake in the northern North Atlantic using shipboard observations, satellite and ocean analysis data. *Deep-Sea Research II*, 56:630–639.

Cox, P.M.; R.A. Betts; C.D. Jones; S.A. Spall; I.J. Totterdell. 2000. Acceleration of global warming due to carbon-cycle feedbacks in a coupled climate model. Nature, 408:184–187.

Culberson, C.H. 1991. Dissolved Oxygen, *WHP Operations and Methods*, July, 1-15.

Dickson, A.G.; C.L. Sabine; and J.R. Christian (eds.) 2007. Guide to Best Practices for Ocean CO_2 Measurements. *PICES Special Publication* 3, 191pp.

Doglioli, A.M.; B. Blanke; S. Speich, and G. Lapeyre. 2007. Tracking coherent structures in a regional ocean model with wavelet analysis: Application to Cape Basin eddies. *Journal of Geophysical Research*, 112(C5):C05043, doi:10.1029/2006JC003952.

Duncombe Rae, C.M.; F.A. Shillington; J.J. Agenbag; J. Taunton-Clark, and M.L. Grundlingh. 1992. An Agulhas ring in the South Atlantic Ocean and its interaction with the Benguela upwelling frontal system. *Deep-Sea Research*, 39:2009–2027.

Faraway, J.J. 2006. Extending the linear model with R: generalized linear, mixed effects and nonparametric regression models. Taylor & Francis Group e-Library Ed., 345 pp.

Garcia, C.A.E. & V.M.T. Garcia. 2008. Variability of chlorophyll-a from ocean color images in the La Plata continental shelf region. *Continental Shelf Research*, 28:1568–1578.

González-Dávila, M.; J.M. Santana-Casiano, and I.R. Ucha. 2009. Seasonal variability of fCO_2 in the Angola-Benguela region. *Progress in Oceanography*, 83:124–133.

Gonzalez-Silvera, A.; E. Santamaria-del-Angel; V.M.T. Garcia; C.A.E. Garcia; R. Mill!an-Nuñez; F. Muller-Karger. 2004. Biogeographical regions of the tropical and subtropical Atlantic Ocean off South America: classification based on pigment (CZCS) and chlorophyll-a (SeaWiFS) variability. *Continental Shelf Research*, 24:983–1000.

Gordon, A.L.; J.R.E. Lutjeharms and M.L. Grondlingh. 1987. Stratification and circulation at the Agulhas Retroflection. Deep-Sea Research, 34(4):565–599.

Goyet C.; F.J. Millero; A. Poisson, and D.K. Shafer. 1993. Temperature dependence of CO_2 fugacity in seawater. *Marine Chemistry*, 44:205–219.

Grasshoff, K.; M. Ehrhardt and K. Kremling. 1999. Methods of seawater analysis. Weinheim, Wiley-VCH, 600p.

Guidi, L.; P.H.R. Calil; S. Duhamel; K.M. Björkman; S.C. Doney; G.A. Jackson; B. Li; M.J. Church; S. Tozzi; Z.S. Kolber; K.J. Richards; A.A. Fong; R.M. Letelier; G. Gorsky; L. Stemmann, and D.M. Karl. Does eddy-eddy interaction control surface phytoplankton distribution and carbon export in the North Pacific Subtropical Gyre? *Journal of Geophysical Research*, 117, G02024, doi:10.1029/2012JG001984.

Hawkins, E. & P.D. Jones. 2013. On increasing global temperature: 75 years after calendar. *Quarterly Journal of the Royal Metereological Society*, 139:1961–1963.

Hales, B.; P.G. Strutton; M. Saraceno; R. Letelier; T. Takahashi; R. Feely; C. Sabine; F. Chavez. 2012. Satellite-based prediction of pCO2 in coastal waters of the eastern North Pacific. *Progress in Oceanography*, 103:1–15.

Ho, D.T.; C.S. Law; M.J. Smith; P. Schlosser; M. Harvey; and P. Hill. 2006. Measurements of air-sea gas exchange at high wind speeds in the Southern Ocean: Implications for global parameterizations. *Geophys. Res. Lett.* 33, L16611, doi:10.1029/2006GL026817.

Hood, E.M.; R. Wanninkhok, and L. Merlivat. 2001. Short timescale variations of fCO_2 in a North Atlantic warm-core eddy: Results from the Gas-Ex 98 carbon interface ocean atmosphere (CARIOCA) buoy data. *Journal of Gephysical Research*, 106(C2):2561–2572.

Hulbert, E.O. 1931. The temperature of the lower atmosphere of the Earth. *Physical Review*, 38:1876–1890.

Hutchings, L., Verheye, H.M., Mitchell-Innes, B.A., Peterson, W.T., Hugget, J.A., Painting, S.J., 1995. Copepod production in the southern Benguela system. ICES Journal Marine Science, 52:439–455.

Hutchintons, L.; C.D. van der Lingen; L.J. Shannon; R.J.M. Crawford; H.M.S. Verheye; C.H. Bartholomae; A.K. van der Plas; D. Louw; A. Kreiner; M. Ostrowski; Q. Fidel; R.G. Barlow; T. Lamont; J. Coetzee; F. Shillington; J. Veitch; J.C. Currie, and P.M.S. Monteiro. 2009. The Benguela Current: An ecosystem of four componentes. *Progress in Oceanography*, 83:15–32.

IPCC Climate Change. 2013. *The Physical Science Basis* (eds Stocker, T.F. *et al.*) 1–33 (IPCC, Switzerland Pub.).

Ito, R.G.; B. Schneider, and H. Thomas2005. Distribution of surface fCO_2 and air–sea fluxes in the Southwestern subtropical Atlantic and adjacent continental shelf. *Journal of Marine System*, 56:227 – 242.

Jiang, L.-Q.; W.-J. Cai; R. Wanninkhof; Y. Wang, and H. Lüger. 2008. Air-sea CO_2 fluxes on the U.S. South Atlantic Bight: Spatial and seasonal variability.*Journal of Geophysical Research*, 113:C07019.

Kanamitsu, M.; W. Ebisuzaki; J. Woollen; S.-K. Yang; J.J. Hnilo; M. Fiorino; G.L. Potter. 2002. NCEP-DOE AMIP-II reanalysis (R-2). Bull. Am. Meteorol. Soc. 83, 1631–1643. The updated data to 2013 were downloaded on 15 July 2014 from /ftp://ftp.cdc.noaa.gov/Datasets/ncep.reanalysis2/gaussian.grid/S.

Koffi, U.; N. Lefèvre; G. Kouadio, and J. Boutin . 2010. Surface CO_2 parameters and air–sea CO_2 flux distribution in the eastern equatorial Atlantic Ocean. *Journal of Marine Systems*, 82:135–144.

Laruelle, G.G.; H.H. Dürr; C.P. Slomp, and A.V. Borges. 2010. Evaluation of sinks and sources of CO_2 in the global coastal ocean using a spatially-explicity typology of estuaries and continental shelves. *Geophysical Research Letters*, 37, L15607, doi:10.1029/2010GL043691.

Lefèvre, N. and A. Taylor. 2002. Estimating pCO_2 from sea surface temperatures in the Atlantic gyres. *Deep-Sea Research I*, 49:539–554.

Lefèvre, N. 2009. Low CO_2 concentrations in the Gulf of Guinea during the upwelling season in 2006. *Marine Chemistry*, 113:93 – 101.

Lentini, C.A.D.; G.J. Goni, and D.B. Olson. 2006. Investigation of Brazil Current rings in the confluence region. *Journal of Geophysical Research*, 111(C6), C06013, doi:10.1029/2005JC002988.

Le Quéré, C., M.R. Raupach, J.G. Canadell, G. Marland *et al.* 2009. Trends in the sources and sinks of carbon dioxide. *Nature Geosc.* 2:831-836.

Le Quéré, C.; G.P. Peters; R.J. Andres; R.M. Andrew; T. Boden; P. Ciais; P. Friedlingstein; R.A. Houghton; G. Marland; R. Moriarty; S. Sitch; P. Tans; A. Arneth; A. Arvanitis; D.C.E. Bakker; L. Bopp; J.G. Canadell; L.P. Chini; S.C. Doney; A. Harper; I. Harris; J.I. House; A.K. Jain; S.D. Jones; E. Kato; R.F. Keeling; K. Klein Goldewijk; A. Körtzinger; C. Koven; N. Lefèvre; A. Omar; T. Ono; G.-H. Park; B. Pfeil; B. Poulter; M.R. Raupach; P. Regnier; C. Rödenbeck; S. Saito; J. Schwinger; J. Segschneider; B.D. Stocker; B. Tilbrook; S. van Heuven; N. Viovy; R. Wanninkhof; A. Wiltshire; S. Zaehle and C. Yue. 2013. Global carbon budget 2013, Earth Syst. Sci. Data Discuss., 6, 689-760, doi:10.5194/essdd-6-689-2013.

Libes, S.M. 2009. Introduction to Marine Biogeochemistry. Academic Press. Second Edition. 909p.

Liss, P.S. & Merlivat, L. 1986. Air-sea gas exchange: Introduction and synthesis. In: P. Buat-Ménard (ed.) The role of air-sea exchange in geochemical cycling. 549 pp.

Liu, K.-K.; L. Atkinson; R. Quinones; L. Talaue-McManu. 2010. Carbon and Nutrient Fluxes in Continental Margins: A Global Synthesis. Springer-Verlag Berlin Heidelberg, 741 pp.

Longhurst, A.; S. Sathyendranath1; T. Platt, and C. Caverhill. 1995. An estimate of global primary production in the ocean from satellite radiometer data. *Journal of Plankton Research*, 17(6):1245–1271.

Lüthi, D., M. Le Floch, B. Bereiter, T. Blunier, J.-M. Barnola, U. Siegenthaler, D. Raynaud, J. Jouzel, H. Fischer, K. Kawamura, and T.F. Stocker. 2008. High-resolution carbon dioxide concentration record 650,000–800,000 years before present. *Nature* 453:379–382.

Lutjeharms, J.R.E. & R.C. Van Ballegooyen. 1988. The retroflection of the Agulhas Current. *Journal of Physical Oceanography*, 18:1570–1583.

Lutjeharms, J.R.E.; F.A. Shillington, and C.M. Duncombe Rae. 1991. Observations of Extreme Upwelling Filaments in the Southeast Atlantic Ocean. *Science*, 253:774–776.

Mahadevan, A.; M. Lèvi; L. Mémey. 2002. Mesoscale variability of sea surface pCO2: What does it respond to? *Global Biogeochemical Cycles*, (PREPRINT), pages 1–7.

McGillicuddy, D.J. & A.R. Robinson. 1997. Eddy-induced nutrient supply and new production in the Sargasso Sea. *Deep-Sea Research I*, 44:1427–1450.

Mendes, C.R.B.; P. Cartaxana, and V. Brotas . 2007. HPLC determination of phytoplankton and microphytobenthos pigments: comparing resolution and sensitivity of a C18 and a C8 method. *Limnology and Oceanography: Methods*, 5:363-370.

Millero, F.J. 2007. The marine inorganic carbon cycle. *Chem. Rev.* 107(2):308–341.

Möller, O.O.Jr.; A.R. Piola; A.C. Freitas; E.J.D. Campos. 2008. The effects of river discharge and seasonal winds on the shelf off southeastern South America. *Continental Shelf Research*, 28(13):1607–1624.

Monteiro, P.M.S. 2010. The Benguela Current System. In: Liu, K.K., L. Atkinson, R. Quinones, L. Talaue-McManus (Eds). Carbon and nutrients fluxes in continental margins: A global synthesis. Springer-Verlag Berlin Heidelberg, 741 pp.

Nardi, E. 2013. Influência do Cone do Rio Grande na Formação de Atividade de Mesoescala na Corrente do Brasil. Dissertação de mestrado. Universidade Federal do Rio Grande.

Neter, J.; W. Wasserman, and M.H. Kutner. 1983. Applied linear regression models. Homewood, IL: Irwin. 667 pp.

Nightingale, P.D., G. Malin, C.S. Law, A.J. Watson, P.S. Liss, M.I. Liddicoat, J. Boutin, and R.C. Upstill-Goddard. 2000. *In situ* evaluation of air-sea exchange parameterizations using novel conservative and volatile tracers. *Global Biogeoch. Cycl.* 14(1):373–387.

Orr, J.C.; E. Maier-Reimer; U. Mikolajewicz; P. Monfray; J.I. Sarmiento; J.R. Toggweiler; N.K. Taylor; J. Palmer; N. Gruber; C.L. Sabine; C. Le Quéré; R.M. Key; J. Boutin. 2001. Estimates of anthropogenic carbon uptake from four three-dimensional global ocean models. *Global Biogeochemical Cycles*, 15:43–60.

Padin, X.A.; M. Vázquez-Rodriguez; M. Castaño; A. Velo; F. Alonzo-Pérez; J. Gago; M. Gilcoto; M. Álvarez; P.C. Pardo; M. de La Paz; A.F. Ríos, and F.F. Pérez. 2010. Air-sea CO2 fluxes in the Atlantic as measured during boreal spring and autumn. *Biogeosciences*, 7:1587–1606.

Peterson, R.G. and L. Stramma. 1991. Upper-level circulation in the South Atlantic Ocean. *Progress in Oceanography*, 26:1–73.

Piontkovski, S.A.; M.R. Landry; Z.Z. Finenko; A.V. Kovalev; R. Williams; C.P. Gallienne; A.V. Mishonov; V.A. Skryabin; Y.N. Tokarev; V.N. Nikolsky. 2003. Plankton communities of the South Atlantic anticyclonic gyre. *Oceanologica Acta*, 26:255–268.

Robinson, C.; A.J. Poulton; P.M. Holligan; A.R. Baker; G. Forster; N. Gist; T.D. Jickells; G. Malin; R. Upstill-Goddard; R.G. Williams; E.M.S. Woodward; M.V. Zubkov. 2006. The Atlantic Meridional Transect (AMT) Programme: A contextual view 1995–2005. *Deep-Sea Research II*, 53:1485–1515.

Sabine C.L., R.A. Feely, N. Gruber, R.M. Key, K. Lee, J.L. Bullster, R. Wanninkhof, C.S. Wong, D.W.R. Wallace, B. Tilbrook, F.J. Millero, T-H. Peng, A. Kozyr, T. Ono, A.F. Rios. 2004. The oceanic sink for anthropogenic CO_2. *Science* 305:367–71.

Santana-Casiano, J.M.; M. González-Dávila, and I.R.Ucha. 2009. Carbon dioxide fluxes in the Benguela upwelling system during winter and spring: a comparison between 2005 and 2006. *Deep-Sea Research II*, 56:533–541.

Saraceno, M. & C. Provost. 2012. On eddy polarity distribution in the southwestern Atlantic. *Deep-Sea Research I*, 69:62–69.

Schimel, D.S.; J.I. House; K.A. Hibbard; P. Bousquet; P. Ciais; P. Peylin; B.H. Braswell; M.J. Apps; D. Baker; A. Bondeau; J. Canadell; G. Churkina; W. Cramer; A. S. Denning; C.B. Field; P. Friedlingstein; C. Goodale; M. Heimann; R.A. Houghton; J.M. Melillo; B. Moore; D. Murdiyarso; I. Noble; S.W. Pacala; I.C. Prentice; M.R. Raupach; P.J. Rayner; R.J. Scholes; W.L. Steffen, and C. Wirth. 2001. Recent patterns and mechanisms of carbon exchange by terrestrial ecosystems. *Nature*, 414:169–172.

Sarmiento, J.L. and N. Gruber. 2002. Sinks for anthropogenic carbon. *Physics Today,* 55:30–36.

Shillington, F.A.; C.J.C. Reason; C.M. Duncombe Rae; P. Florenchie and P. Penven. 2006. Large scale physical variability of the Benguela Current Large Marine Ecosystem (BCLME). In: *Large Marine Ecosystem*, Vol. 14. Eds. V. Shannon, G. Hempel, P. Malanotte-Rozzoli, C. Moloney and J. Woods. Ed. Elselvier, 410 pp.

Siegel, D.A.; P. Peterson; D.J. McGillicuddy Jr.; S. Maritorena, and N.B. Nelson. 2011. Bio-optical fottprint created by mesoscale eddies in the Sargasso sea. *Gephysical Research Letters*, 38, L13608, doi:10.1029/2011GL047660.

Signorini, S.R.; A. Mannino; R.G. Najjar Jr.; M.A.M. Friedrichs; W.-J. Cai; J. Salisbury; Z. Aleck Wang; H. Thomas, and E. Shadwick. 2013. Surface ocean pCO_2 seasonality and sea-air CO_2 flux estimates for the North American east coast. *Journal of Geophysical Research: Oceans*, 118:1–22, doi:10.1002/jgrc.20369.

Stramma, L. 1989. The Brasil Current transport south of 23˚S. *Deep Sea Research*, 36:639–646.

Stramma, L. & M. England. 1999. On the water masses and mean circulation of the South Atlantic Ocean. *Journal of Geophysical Research*, 104, C9, 20863–20883.

Takahashi, T. 1961. Carbon dioxide in the atmosphere and in the Atlantic Ocean. *Journal of Geophysical Research,* 66(2):477–494.

Takahashi, T.; R.A. Feely; R.F. Weiss; R.H. Wanninkhof; D.W. Chipman; S.C. Sutherland and T.T. Takahashi. 1997. Global air-sea flux of CO_2: An estimate based on measurements of sea–air pCO_2 difference. *Proc. Natl. Acad. Sci. USA,* 94:8292–8299.

Takahashia,T.; S.C. Sutherland; C. Sweeney; A. Poisson; N. Metzl; B. Tilbrookc; N. Bates; R. Wanninkhof; R.A. Feely; C. Sabine; J. Olafsson; Y. Nojiri. 2002. Global sea–air CO_2 flux based on climatological surface ocean pCO_2, and seasonal biological and temperature effects. Deep-Sea Research II, 49:1601–1622.

Takahashi, T., S.C. Sutherland, R. Wanninkhof, C. Sweeney, R.A. Feely, D.W. Chipman, B. Hales,G. Friederich, F. Chavez, C. Sabine, and others. 2009. Climatological mean and decadal change in surface ocean pCO_2, and net sea-air CO_2 flux over the global oceans. *Deep Sea Research Part II* 56(8–10):554–577.

Tans, P. & R. Keeling. 2014. Trends in atmospheric carbon dioxide, NOAA/ESRL (www.esrl.noaa.gov/gmd/ccgs/trends/) and Scripps Institute of Oceanography (scrippsco2.ucsd.edu/). http://www.esrl.noaa.gov/gmd/ccgg/trends, ultimo acesso em 11 de julho de 2014.

Ternon, J.F.; C. Oudot; A. Dessier, and D. Diverres. 2000. A seasonal tropical sink for atmospheric CO_2 in the Atlantic ocean: the role of the Amazon River discharge. *Marine Chemistry*, 68:183–201.

Triola, M.F. 2008. Introdução à estatística. Ed. LTC – Livros Técnicos e Científicos Editora S.A., 696 pp.

Tsunogai, S.; S. Watanabe; T. Sato. 1999. Is there a continental “continental shelf pump” for the absorption of atmospheric CO_2? *Tellus*, 51B:701–712.

Valentin, J.L. 2000. Ecologia numérica: uma introdução a análise multivariada de dados ecológicos. Ed. Interciência, 117 pp.

Wanninkhof, R. 1992. Relationship between wind speed and gas exchange over the ocean. *J. Geophys. Res.* 97(C5):7373–7382.

Wanninkhof, R. & McGillis, W.R. 1999. A cubic relationship between air-sea CO_2 exchange and wind speed. *Geophys. Res. Lett.* 26(13):1889–1892.

Weiss, R.F. 1974. Carbon dioxide in water and seawater: the solubility of a non-ideal gas. *Marine Chemistry*, 2:203–215.

Weiss, R.F. & B.A. Price. 1980. Nitrous oxide solubility in water and seawater. *Marine Chemistry*, 8:347–359.

Zapata M.; F. Rodríguez, and J.L. Garrido. 2000. Separation of chlorophylls and carotenoids from marine phytoplankton: a new HPLC method using a reversed phase C8 column and pyridine-containing mobile phases. *Marine Ecology Progress Series*, 195:29-45.

Zuur, A.F.; E.N. Ieno; N.J. Walker; A.A. Saveliev; G.M. Smith. 2009. Mixed effects models and extentions in ecology with R. Springer Ed., 564 pp.